Detailed modeling of the atmospheric degradation mechanism of very-short lived brominated species

Gisèle Krysztofiak, Valéry Catoire, Gilles Poulet, Virginie Marécal, Michel Pirre, Florent Louis, Sébastien Canneaux, Béatrice Josse

HAL Id: insu-00877474

https://insu.hal.science/insu-00877474

Submitted on 28 Oct 2013

Detailed modeling of the atmospheric degradation mechanism

of very-short lived brominated species

G. Krysztofiak[a], V. Catoire[a,*], G. Poulet[a], V. Marécal[b], M. Pirre[a], F. Louis[c], S. Canneaux[c], B. Josse[b]

[a] Laboratoire de Physique et Chimie de l'Environnement et de l'Espace (LPC2E), CNRS - Université d'Orléans (UMR 6115), 45071 Orléans cedex 2, France

[b] Centre National de Recherches Météorologiques - Groupe d'études de l'Atmosphère Météorologique (CNRM-GAME), Météo-France - CNRS (URA 1357), 31057 Toulouse cedex 1, France

[c] PhysicoChimie des Processus de Combustion et de l'Atmosphère (PC2A) CNRS - Université Lille 1 Sciences et Technologies (UMR 8522), 59655 Villeneuve d'Ascq Cedex, France

*Corresponding author: Valery.Catoire@cnrs-orleans.fr

Atmospheric Environment.

Abstract

Detailed chemical reaction schemes for the atmospheric degradations of the very short-lived species (VSLS) bromoform ($CHBr_3$) and dibromomethane (CH_2Br_2) have been established. These degradation schemes have been implemented in the meteorological/tracer transport model CATT-BRAMS used in the present case as pseudo one-dimensional model with chemistry of CH_4, CO, HO_x, NO_x, NO_y and O_x. They include the main possible reactions of the intermediate brominated peroxy radicals RO_2 (with R = CH_2Br, $CHBr_2$ and CBr_3) for which the most likely reaction pathways with HO_2 have been found using *ab initio* computational calculations. The full degradation schemes have been run for two well-defined realistic scenarios, "clean" atmosphere and "moderately" NO_y-polluted atmosphere, as representative of a tropical coastal region where these VSLS natural emissions are expected to be important. The Henry's law constants of the brominated organics products have been estimated by using the Bond Contribution Method (BCM; Meylan and Howard, 1991) or the Molecular Connectivity Index (MCI; Nirmalakhandan and Speece, 1988). Using these constants, the least soluble species formed from the VSLS degradation are found to be CBr_2O,

CHBrO, $CBr_3O_2NO_2$, $CHBr_2O_2NO_2$, BrO, $BrONO_2$ and HOBr, which leads those to be potentially transported into the tropical tropopause layer (TTL) in case of deep convection and contribute to stratospheric bromine additionally to the original substances. For bromoform and dibromomethane degradation, the moderate NO_y pollution increases the production of the least soluble species and thus approximately doubles the bromine quantity potentially able to reach the TTL (from 22.5% to 43% for $CHBr_3$ and from 8.8% to 20.2 % for CH_2Br_2). The influence of the reactions of the RO_2 radicals with HO_2, CH_3O_2 and NO_2 on the nature and abundance of the stable intermediate and end-products has been tested for $CHBr_3$ degradation. As a result, the reactions of the RO_2 radicals with NO_2 have no impact. Taking into account the reaction between RO_2 and CH_3O_2 and modifying the branching ratios of the reaction between RO_2 and HO_2 lead to a small impact on the bromoform degradation by slightly decreasing (by 10%) the bromine quantity potentially able to reach the TTL. As a final point, in contrast to $CHBr_3$, CH_2Br_2 degradation produces negligible quantities of organics species and the effects of pollution increase only the inorganic species production. By taking into account the results of these tests, new simplified degradation schemes for $CHBr_3$ and CH_2Br_2 are proposed.

1.   Introduction

Until the beginning of the 21st century, stratospheric ozone depletion has been exclusively explained by reactions of active halogen gases with ozone. The active halogen gases originated from long-lived species such as chlorofluorocarbons (CFCs) for chlorine, and halons and CH$_3$Br for bromine. Recent measurements of total stratospheric inorganic bromine, Br$_y$ (Dorf et al., 2008), and their comparison with the measurements of bromine derived from halons and CH$_3$Br showed significant discrepancies (Montzka and Reimann et al., 2011). Actually bromine-containing long-lived species are not the single source of stratospheric inorganic bromine as very short-lived species (VSLS) also contribute (Ko and Poulet et al., 2003; Law and Sturges et al., 2007; Montzka and Reimann et al., 2011). These VSLS are substances with atmospheric lifetime shorter than six months, which is generally too short to reach the stratosphere. However, they may enter the tropical tropopause layer (TTL) into the tropical region by deep convection, and then the stratosphere by slow radiative ascent for air having reached at least the level of zero radiative heating (LZRH, ~15.5 km or 360 K). Convection can lift VSLS, in the form of their source gases (SGs) or their low solubility product gases (PGs) within a few hours from the boundary layer into the TTL. In the tropics, VSLS are mainly emitted by natural marine sources from warm tropical oceans (Hense and Quack, 2009). Bromoform (CHBr$_3$) and dibromomethane (CH$_2$Br$_2$) are the most abundant brominated short-lived SGs, with a global mean lifetime of 26 days and 120 days, respectively (Ko and Poulet et al., 2003). Research is now focused on the contribution of VSLS to stratospheric bromine by using modeling calculations (Kerkweg et al., 2008; Brioude et al., 2010; Pisso et al., 2010; Aschmann et al., 2009; Hossaini et al., 2010), balloon-borne measurements (Dorf et al., 2008) and satellite measurements (Sinnhuber et al., 2005). This contribution is found to be largely uncertain, varying from less than 1 part per trillion volume (pptv) mixing ratios up to more than 8 pptv. Most models use simple degradation schemes for the VSLS, which do not consider the intermediates organic PGs as particular species with their own physical properties (e.g., solubility) and reactivity toward other atmospheric species. Only one detailed chemical scheme for degradation of CHBr$_3$ and CH$_2$Br$_2$ has been proposed, by Hossaini et al. (2010). They used a chemistry reaction scheme in the three dimensional (3D) TOMCAT/SLIMCAT global chemistry transport model and concluded on the small influence of the organic products on the global scale. Nevertheless, neither study considered all the possible degradation pathways.

The aim of this paper is firstly to propose a full degradation scheme of bromoform and dibromomethane and to implement it in a meteorological/tracer transport model (CATT-BRAMS; Freitas et al., 2009) used as a pseudo one dimensional model with the atmospheric chemistry of CH_4, CO, HO_x, NO_x, NO_y and O_x. The computations are made under high sunlight conditions as those prevailing in the tropical regions.

The atmospheric removal of $CHBr_3$ and CH_2Br_2 is mainly initiated via reaction with OH radical and photolysis. In the presence of molecular oxygen, the first step (either OH- or Cl-oxidation reaction, or photolysis) leads to the formation of organic brominated peroxy radicals RO_2 (with R = CH_2Br, $CHBr_2$ or CBr_3). The chemistry of peroxy radicals closely depends on the conditions of pollution and in particular on the level of nitrogen oxides (NO_x). In regions with high NO_x levels, the chemistry of RO_2 radicals is essentially governed by the reactions with NO, which lead to the exclusive formation of the alkoxy radical (RO) and NO_2 for bromine and small size compounds (Mc Givern et al., 2004; Wallington et al., 1997). However, it is also interesting to study the importance of the reactions between RO_2 and NO_2, giving alkyl peroxy nitrates (RO_2NO_2), compared to the RO_2 + NO reactions. Indeed, species such as $CH_3O_2NO_2$ are rather unstable, but the substitution of one or more H atoms by halogen atoms leads to much longer thermal lifetimes (Kirchner et al., 1998, Köppenkastrop et al., 1991). Consequently, halogenated alkyl peroxy nitrates might be temporary reservoirs for peroxy radicals. In regions with low NO_x levels (less than few tens of pptv) such as the marine atmosphere, the degradation of peroxy radicals also involves the cross reactions RO_2 + HO_2 and RO_2 + $R'O_2$, where $R'O_2$ represents the most abundant atmospheric organic peroxy radicals, i.e. mainly CH_3O_2, $C_2H_5O_2$ and $CH_3C(O)O_2$. In particular CH_3O_2 can reach concentrations as high as HO_2 concentrations (Villenave and Lesclaux, 1996) so that the RO_2 + CH_3O_2 reaction may need to be considered as a significant degradation pathway (Tyndall et al., 2001). Moreover, these cross reactions between peroxy radicals potentially lead to several different products. The reactions between alkyl RO_2 and HO_2 proceed via the formation of a short-lived tetroxide intermediate ROOOOH, which decomposes to form different products (Wallington et al., 1997). In most cases, the major product is the hydroperoxide RO_2H. However, for halogenated peroxy radicals, other final products arise, with yields depending on the nature and the number of the halogen atoms in the RO_2 species (Lesclaux et al., 1997). Another question to properly close the degradation scheme is the fate of the species produced by the RO_2 radical reactions, which can undergo washout (depending on their solubility), photolysis, or react with OH (or Cl) to form inorganic bromine species (Br_y) as end-products.

The second goal of this paper is to study the influence of these different parameters, i.e. the oxidant concentration, the level of NO_x pollution and the relative importance of the different peroxy radical cross reactions, on the final chemical product distribution. Especially, the different mechanisms discussed above, the partitioning between the different PGs (organics and inorganics) produced in the lower atmosphere and the ability of these PGs to reach the TTL in the case of convection are studied. For that, the solubility of each species is determined by attributing an individual Henry's law constant and only the least soluble species are considered to potentially reach the TTL. As a conclusion, the importance of each reaction is discussed and simplified chemical schemes of VSLS degradation are established, to be more conveniently used in future simulations.

This paper is organized as follows: Section 2 gives a detailed chemical degradation scheme for bromoform and dibromomethane. Section 3 describes the atmospheric model used for this study and Section 4 presents the results and the discussion of the atmospheric simulations.

2.   Chemical mechanisms for the atmospheric degradations of $CHBr_3$ and CH_2Br_2

This section presents the different degradation pathways of the main bromine VSL source gases, bromoform ($CHBr_3$) and dibromomethane (CH_2Br_2) in the atmosphere, and tools to establish, on the one hand, the chemical scheme and, on the other hand, the solubility of the brominated products. The mechanism is based on the general scheme of the halomethane degradation proposed by Ko and Poulet et al. (2003). The removal of bromine SGs occurs via OH and Cl reactions and photolysis. The peroxy radicals (RO_2) produced in the first oxidation steps can react with species such as NO, NO_2, HO_2 and CH_3O_2 to form aldehydes, hydroperoxides and alcohols as intermediate organic products.

The reaction scheme of peroxy radicals are complex and depend on the atmospheric conditions, in particular on the NO_x concentration (Tyndall et al., 2001). When the abundance of NO_x is high (more than a few parts per billion volume mixing ratios (ppbv)), the fate of peroxy radicals is dominated by their reaction with NO. Under conditions of low NO_x levels (less than few tens of pptv), the cross-reactions of RO_2 with CH_3O_2 or HO_2 dominate with respect to the reaction with NO. When the abundance of NO_x is moderated (from few tens of pptv to some ppbv), all these reactions are in competition. Finally, the oxidation scheme of

VSLS terminates by reactions of the intermediate products with OH and photodissociations, leading to inorganic bromine production.

The atmospheric reaction mechanisms of analogous chlorinated peroxy radicals, especially the reactions between RO_2 and HO_2, are well known from laboratory studies (Catoire et al., 1994; Catoire et al., 1996; Wallington et al., 1997) or from computational calculations (Hou et al., 2005), whereas this is not the case for brominated peroxy radical reactions. Consequently, computational calculations have been performed to help establishing the most likely chemical mechanisms by determining the standard reaction enthalpies of RO_2 + HO_2 reactions. The computational methods and the estimations of Henry's law constants are explained below, before presenting the detailed mechanisms of the atmospheric degradation of the VSLS.

2.1.   Computational methods for the estimation of the standard reaction enthalpies at 298 K of the RO_2 + HO_2 reaction

In order to determine the energetically most favorable reaction pathways for the cross reactions RO_2 + HO_2, *ab initio* calculations of the standard reaction enthalpies have been performed. All calculations used the GAUSSIAN03 (Frisch et al., 2004) and GAUSSIAN09 (Frisch et al., 2009) software packages. Geometric parameters were fully optimized with the second Møller-Plesset perturbation method (Møller and Plesset, 1934) combined with the Dunning's correlation consistent basis set cc-pVTZ (Dunning et al., 1989; Kendall et al., 1992; Woon et al., 1993; Peterson et al., 1994; Wilson et al., 1996). Scaled vibrational frequencies and scaled Zero-Point Energies (ZPE) were determined within the harmonic approximation at the same level of theory as that for geometries. The *ab initio* vibrational frequencies were multiplied by an appropriate scaling factor (0.95) (Johnson, 2011). Electronic energies were obtained employing the single and double coupled cluster theory with inclusion of a perturbative estimation for triple excitation (CCSD(T)) (Cizek et al., 1969; Pople et al., 1987; Purvis et al., 1982; Scuseria et al., 1988; Scuseria et al., 1989) with the aug-cc-pVTZ basis set. The frozen-core approximation has been applied to the CCSD(T) calculations. This means that the inner shells are excluded when estimating the correlation energy. Though the CCSD(T) approach is considered as a "golden standard", providing a good balance between cost and accuracy, it is still possible to improve the coupled cluster energies estimating the effects of higher excitations, i.e. the full configuration-interaction energies as proposed by Goodson (2002). This is referred to as continued fraction approximation (cf). We applied the cf-correction in the energetics of the studied reactions.

Reaction enthalpies at 298 K were computed using the KISTHEP program (Henon et al., 2003). The BSSE was not considered here because the common counterpoise correction is estimated to be relatively small for a large basis set involving diffuse functions such as the aug-cc-pVTZ basis set and for reaction enthalpies involving species which are neither adducts nor Van der Waals molecular complexes. Table 1 lists the reaction enthalpies $\Delta_r H°$ at 298 K calculated at the CCSD(T)/aug-cc-pVTZ//MP2/cc-pVTZ level of theory with and without the cf-correction. As shown in Table 1, there is little influence of the cf-correction on the calculated reaction enthalpies at 298 K (< 0.9 kcal mol^{-1}) demonstrating the convergence of the reported values.

The results obtained indicate that the reactions between CH_2BrO_2, $CHBr_2O_2$, CBr_3O_2 radicals and HO_2 are strongly exothermic with the exception of the reaction pathways (6b'), (20b') and (35b'). The exothermicity is observed to increase with increasing bromine substitution of the reactant. Our calculated values of $\Delta_r H°_{298K}$ for reaction pathways (6a), (6b'), (20a), (20b'), (35a), (35b') are in good agreement with the values obtained by McGivern et al. (2004) at a different level of theory (CCSD(T)/cc-pVTZ//MP2(Full)/6-311+G(d)). Interestingly, our results are also in very good agreement with the calculations of Hou et al. (2005) for the channels (a), (b), (b') and (c) of the analogous chlorine compounds The chemical model, established in the next sections, takes into account all these results.

2.2. Estimation methods for the Henry's law constants

The halogenated organic intermediate products are more or less soluble. The Henry's law constants are not known for complex halogenated species. Consequently, we used the Bond Contribution Method (BCM) (Meylan and Howard, 1991) or the Molecular Connectivity Index (MCI) method (Nirmalakhandan and Speece, 1988) to estimate them. These methods attribute a "contribution value" for each different atom and/or each bond present in the molecule, depending on their chemical nature, and estimate the Henry's law constant from these values.

Meylan and Howard (1991; BCM) attributed a contribution value for each bond in the molecule (C-C, C-H, C-O, C-Br…) and applied some correction factors to certain chemical classes (alcohols, cyclic alkane …). By summing all the contribution values, the log water to air partition coefficient (LWAPC) is found, which corresponds to the decimal logarithm of the unitless Henry' law constant $k°_H$ in the chemical equilibrium for a given species A defined by the dimensionless ratio of the species concentrations in the two phases:

A (gas) ↔ A (liquid) with $k°_H = C_{A(liq)}/ C_{A(gas)}$

Usually, the Henry' law constant is defined as $k°_H = C_{A(liq)} / P_{A(gas)}$, where $C_{A(liq)}$ and $P_{A(gas)}$ are the concentration of the species in the liquid phase and the partial pressure in the gas phase in units of mol L^{-1} and atm, respectively. The unitless Henry' law constant is converted into mol L^{-1} atm^{-1} by dividing by the temperature (298 K) and the gas constant (8.205746×10^{-2} L mol^{-1} atm K^{-1}).

Nirmalakhandan and Speece (1988; MCI) developed an equation to estimate the unitless Henry's law constants taking into consideration three different parameters: the polarizability parameter, the molecular connectivity index and the hydrogen bonding index. The polarizability parameter is calculated from the different atoms (C, H, Br…) and functions (aldehyde, ketone…) present in the molecule, the molecular connectivity index characterizes the bond in the molecule and the hydrogen bonding index is equal to 1 if the molecule contains an electronegative element attached directly to a carbon atom holding a hydrogen atom.

Before estimating the Henry's law constant of our bromine products, we have tested the two methods by comparisons with well-known Henry's law constants (referenced by Sander et al., 1999). Table 2 shows these comparisons. For small peroxides and alcohols, BCM is better than MCI method, which overestimates the values for peroxides and underestimates them for alcohols. So we used this method for brominated peroxides and alcohols ($CH_nBr_{3-n}OOH$ and $CH_nBr_{3-n}OH$, with n = 0, 1, or 2). Both methods are in excellent agreement for the estimation of aldehydes and ketones Henry's law constants. However, BCM estimates the constant from the bond between each atom and treats carbonyl groups (C=O) as single atoms. Their authors (Meylan and Howard, 1991) established the values of each bond but with no value for the bond CO-Br. MCI method uses the contribution of each atom of the molecule, i.e. C, O and Br as single atoms, and moreover considers aldehydes and ketones as subgroups of the molecule for which an additional contribution to the Henry's law constant is attributed. Consequently MCI enables the estimate of Henry's law constants for brominated aldehydes or ketones, and we used this method in this case. These two estimation methods allowed us to derive an order of magnitude value for the Henry's law constants. The results of the estimated Henry's law constants for the bromine compounds present in our model are reported in Table 3. The most soluble organic species are CBr_3O_2H, $CHBr_2O_2H$, CBr_3OH and $CHBr_2OH$ with Henry law's constants higher than 10^4 mol L^{-1} atm^{-1}, whereas the least soluble organics are CBr_2O, $CHBrO$ and the brominated methyl peroxynitrates (RO_2NO_2) with constants lower than 10^3 mol L^{-1} atm^{-1}. Note that HBr is very soluble, even

with a very low Henry's law constant, but with a high acidity constant ($K_a = 10^9$) leading to a high effective constant (Yang et al., 2005). Seinfeld and Pandis (2006) proposed that species with Henry's law constants lower than 10^3 mol L^{-1} atm^{-1} are considered less soluble, whereas species with constants between 10^3 and 10^4 mol L^{-1} atm^{-1} are moderately soluble and species with constants higher than 10^4 mol L^{-1} atm^{-1} are very soluble. For our study, we considered only two classes: species with constants higher than 10^4 mol L^{-1} atm^{-1} as very soluble, and species with constants lower than 10^4 mol L^{-1} atm^{-1} as less soluble, so HOBr, CH_2BrO_2H and CH_2BrOH join the latter group. Indeed, for a cloud with a typical liquid water content of 1 g m^{-3} of air (Seinfeld and Pandis, 2006), a constant of 10^4 mol L^{-1} atm^{-1} corresponds to a mass aqueous fraction of 20%.

2.3. Bromoform degradation mechanism

In the atmospheric degradation of CHBr$_3$, the first step is either the reaction with OH, Cl or photolysis. The different pathways, oxidation or photolysis, do not form the same intermediate products (CBr$_3$O$_2$ and CHBr$_2$O$_2$). According to Ko and Poulet et al. (2003), CHBr$_3$ is the only brominated VSLS (with CHBr$_2$Cl) for which photolysis is as important as the reaction with OH, by comparison with other VSLS for which OH oxidation dominates.

2.3.1. OH- or Cl-initiated oxidation of CHBr$_3$

The oxidation of CHBr$_3$ by OH or Cl (Ko and Poulet, 2003 and reference therein; Kamboures et al., 2002) leads to H-abstraction to form CBr$_3$ radical, which is rapidly converted into CBr$_3$O$_2$ radical in the presence of ambient oxygen:

$$CHBr_3 + OH + O_2 \rightarrow CBr_3O_2 + H_2O \tag{1}$$

$$CHBr_3 + Cl + O_2 \rightarrow CBr_3O_2 + HCl \tag{2}$$

Then, depending on the atmospheric conditions the brominated peroxy radical may react with NO, NO$_2$, HO$_2$ and CH$_3$O$_2$. The reaction of CBr$_3$O$_2$ with NO leads exclusively to CBr$_3$O radical (Mc Givern et al., 2002 and 2004; Wallington et al., 1997), which dissociates rapidly by Br-elimination, by analogy with CH$_2$BrO (Chen et al., 1995; Orlando et al., 1996):

$$CBr_3O_2 + NO \rightarrow CBr_3O + NO_2 \tag{3}$$

$$CBr_3O \rightarrow CBr_2O + Br \tag{4}$$

The reaction of peroxy radicals with NO$_2$ proceeds exclusively via a termolecular recombination reaction (Wallington et al., 1997):

$$CBr_3O_2 + NO_2 + M \leftrightarrow CBr_3O_2NO_2 + M \tag{5}$$

The reaction between CBr_3O_2 and HO_2 leads to formation of the hydroperoxide CBr_3O_2H and/or the ketone CBr_2O:

$$CBr_3O_2 + HO_2 \rightarrow CBr_3O_2H + O_2 \tag{6a}$$

$$CBr_3O_2 + HO_2 \rightarrow CBr_2O + HOBr + O_2 \tag{6b}$$

Mc Givern et al. (2004) considered another pathway (6b') corresponding to a different geometry of the tetroxide intermediate (ROOOOH), but with one same final product (CBr_2O) as (6b) after rapid Br-elimination from CBr_3O:

$$CBr_3O_2 + HO_2 \rightarrow CBr_3O + OH + O_2 \tag{6b'}$$

The similar reactions for chlorinated peroxy radicals have been well studied by experimental means under laboratory conditions by Catoire et al. (1994) and Catoire et al. (1996) and by theoretical calculations by Hou et al. (2005), leading to kinetic data (rate parameters and branching ratios for the pathways). The brominated organic peroxy radical reactions have only been studied by Mc Givern et al. (2004) using theoretical Rice-Ramsperger-Kassel-Marcus (RRKM) calculations, but these authors did not consider all the possible pathways as Hou et al. (2005) did for chlorinated compounds. Our calculations of the reaction enthalpies, presented in Section 2.1, for the reactions (6a), (6b) and (6b') are in good agreement with the work of these authors for the brominated and chlorinated peroxy radicals, as detailed in Section 2.1 and shown in Table 1. The experimental results of Catoire et al. (1996) for the equivalent reaction of chlorine compounds showed that CCl_2O is the single product under laboratory conditions. They observed the production of HOCl, suggesting that pathway (b) is the main pathway. However, our theoretical results, consistent with the previous ones reported above, suggest that CBr_3O_2H (from pathway (a)) and $CBr_2O + HOBr$ (from pathway (b)) are the main products of the reaction between CBr_3O_2 and HO_2, being the more exothermic reactions. In addition, according to Hou et al. (2005), for the study of chlorinated compounds, the main product is CCl_3O_2H due to the lower potential energy barrier of reaction (a) than (b), in addition to its significant exothermicity. They explain the experimental results of Catoire et al. (1996) by the fact that pathway (a) for chlorine (forming CCl_3O_2H) is exothermic enough (-44.2 kcal mol^{-1}) to allow for the dissociation of CCl_3O_2H into CCl_2O and HOCl (needing 38 kcal mol^{-1}). Therefore, by analogy with chlorine, we consider the branching ratio for reaction (6a) to be $k_{6a}/k_6 = 1$.

Finally, the cross reaction between CBr_3O_2 and CH_3O_2 may occur via two different pathways (Wallington et al., 1992; Shallcross et al., 2005):

$$CBr_3O_2 + CH_3O_2 \rightarrow CBr_2O + Br + CH_2O + HO_2 \tag{7a}$$

$$CBr_3O_2 + CH_3O_2 \rightarrow CBr_3OH + CH_2O + O_2 \tag{7b}$$

In fact, in a first step channel (7a) produces two alkoxy radicals, CBr_3O and CH_3O, which rapidly form carbonyl dibromide CBr_2O (by Br-atom elimination) and formaldehyde CH_2O (by reaction with O_2), respectively. Channel (7b) leads to perbrominated methanol (CBr_3OH) and formaldehyde. For the analogous chlorine cross reaction ($CCl_3O_2 + CH_3O_2$) the experimental branching ratio k_{7a}/k_7 was indirectly found to be 0.5 ± 0.2 (Catoire et al., 1996). These reactions are not documented for brominated compounds, so we chose to follow the indication of Madronich et al. (1990) who proposed a method to estimate the branching ratios for the cross reaction ($CH_3O_2 + CBr_3O_2$) from the self reactions of the two reactants of the cross reaction, here CH_3O_2 and CBr_3O_2. The self reaction of CH_3O_2 occurs via two pathways with branching ratios different from zero, $k_{8a}/k_8 = 0.4$ and $k_{8b}/k_8 = 0.6$ (Tyndall et al., 1998):

$$CH_3O_2 + CH_3O_2 \rightarrow 2\ CH_3O + O_2 \tag{8a}$$

$$CH_3O_2 + CH_3O_2 \rightarrow CH_3OH + CH_2O + O_2 \tag{8b}$$

Most of the self reactions of the halogenated peroxy radicals, such as $CF_2ClCH_2O_2$, $CFCl_2CH_2O_2$ (Tuazon et al., 1994), CH_3CHClO_2 (Maricq et al., 1993), CH_2ClO_2 and $CHCl_2O_2$ (Niki et al., 1980; Catoire et al., 1996) and CCl_3O_2 (Catoire et al., 1996), occur exclusively via one pathway:

$$RO_2 + RO_2 \rightarrow 2\ RO + O_2 \tag{9}$$
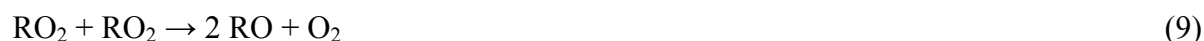
with R being this time the substitute organic radical. So we use $k_{9a}/k_9 = 1.0$. If we apply the method of simple averaging from Madronich et al. (1990) in our cases, we find $k_{7a}/k_7 = 0.7$ and $k_{7b}/k_7 = 0.3$, which we used for our simulations.

Overall the above reactions implying CBr_3O_2 produce four brominated organics products: CBr_2O, $CBr_3O_2NO_2$, CBr_3O_2H and CBr_3OH. These compounds are more or less hydrosoluble and their Henry's law constants have been evaluated in Section 2.2.

Other possible sinks in the atmosphere are gas phase reactions:

- for CBr_2O (Libuda et al., 1991):

$$CBr_2O + h\nu \rightarrow CO + 2\ Br \tag{10}$$

- for $CBr_3O_2NO_2$, based on analogous chlorinated compounds (Köppenkastrop and Zabel, 1991):

$$CBr_3O_2NO_2 + M \rightarrow CBr_3O_2 + NO_2 + M \tag{11}$$

and by analogy with $CH_3O_2NO_2$ (Atkinson et al., 2006):

$$CBr_3O_2NO_2 + h\nu \rightarrow CBr_3O_2 + NO_2 \tag{12a}$$

$$CBr_3O_2NO_2 + h\nu \rightarrow CBr_2O + Br + NO_3 \tag{12b}$$

- for CBr_3O_2H, based on the reaction of CH_3O_2H (Atkinson et al., 2006):

$$CBr_3O_2H + h\nu \rightarrow CBr_2O + Br + OH \qquad (13)$$

$$CBr_3O_2H + OH \rightarrow CBr_3O_2 + H_2O \qquad (14)$$

- for CBr_3OH:

$$CBr_3OH + OH \rightarrow CBr_2O + Br + H_2O \qquad (15)$$

The overall reaction scheme discussed in this section is summarized in Fig. 1 and all kinetic data used are given in Table 4. The references for the chosen kinetic data are detailed in Section 3.

2.3.2. Photolysis of CHBr₃

The photolysis of $CHBr_3$ leads to the direct elimination of a Br atom and the formation of the peroxy radical $CHBr_2O_2$:
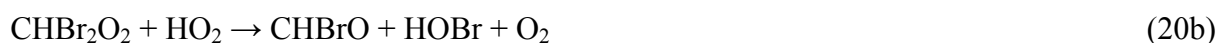
$$CHBr_3 + h\nu \rightarrow CHBr_2O_2 + Br \qquad (16)$$

Similarly to CBr_3O_2, $CHBr_2O_2$ reacts with NO to form $CHBr_2O$ (Mc Givern et al., 2004; Wallington et al., 1997) and then CHBrO:

$$CHBr_2O_2 + NO \rightarrow CHBr_2O + NO_2 \qquad (17)$$

$$CHBr_2O \rightarrow CHBrO + Br \qquad (18)$$

The termolecular reaction of $CHBr_2O_2$ with NO_2 also occurs:

$$CHBr_2O_2 + NO_2 + M \leftrightarrow CHBr_2O_2NO_2 + M \qquad (19)$$

For the reaction between $CHBr_2O_2$ and HO_2 three pathways may take place:

$$CHBr_2O_2 + HO_2 \rightarrow CHBr_2O_2H + O_2 \qquad (20a)$$

$$CHBr_2O_2 + HO_2 \rightarrow CHBrO + HOBr + O_2 \qquad (20b)$$
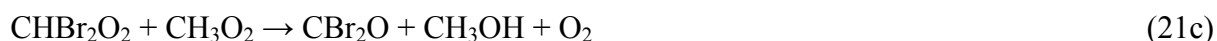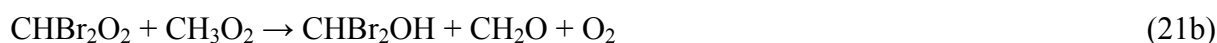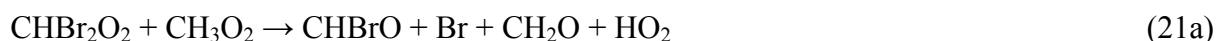
$$CHBr_2O_2 + HO_2 \rightarrow CBr_2O + H_2O + O_2 \qquad (20c)$$

As previously, Mc Givern et al. (2004) considered another pathway corresponding to a different geometry in the intermediate:

$$CHBr_2O_2 + HO_2 \rightarrow CHBr_2O + OH + O_2 \qquad (20b')$$

Mc Givern et al. (2004) studied only pathways (a) and (b'), giving branching ratios of 0.59 and 0.41, respectively. But they did not consider pathway (c), as suggested by Wallington et al. (1996) for chlorinated compounds, which forms carbonyl dibromide CBr_2O. Our calculations of reaction enthalpies (Section 2.1) give results similar to those for chlorinated compounds found by Hou et al. (2005), as shown in Table 1. As explained previously, the cross reaction proceeds via a tetroxide intermediate ROOOOH, and depending on the geometry of this tetroxide, the final products are different (pathways a, b or b', c). As previously stated (Section 2.3.1), Hou et al. (2005) found $CHCl_2O_2H$ as the main product in their study of the analogous chlorinated compound reaction, due to the exothermicity and the
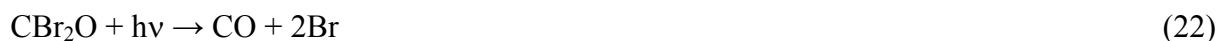
lower potential energy barrier of channel (a) with respect to channels (b) and (c), and explained the non observation of $CHCl_2O_2H$ in the experimental results of Catoire et al. (1996) by the decomposition of $CHCl_2O_2H$ into CHClO. The branching ratios found for chlorinated compounds by Catoire et al. (1996) were $k_{20b}/k_{20} = 0.7$ and $k_{20c}/k_{20} = 0.3$. By analogy, assuming $CHCl_2O_2H$ is totally converted into CHClO, due to the exothermicity of reaction (a) for chlorinated compounds, i.e. the reaction proceeds mainly through channel (20a) and the realistic branching ratio would be $k_{20a}/k_{20} = 0.7$ and $k_{20c}/k_{20} = 0.3$. Consequently, for the brominated compounds, we set $k_{20a}/k_{20} = 0.7$ and $k_{20c}/k_{20} = 0.3$.

The reaction between $CHBr_2O_2$ and CH_3O_2 can proceed via three pathways. According to the estimation method of Madronich et al. (1990) again, we can approximate the branching ratio of the cross reaction, $k_{21a}/k_{21} = 0.7$ and $k_{21b}/k_{21} = 0.3$ and $k_{21c}/k_{21} = 0$:

$$CHBr_2O_2 + CH_3O_2 \rightarrow CHBrO + Br + CH_2O + HO_2 \tag{21a}$$
$$CHBr_2O_2 + CH_3O_2 \rightarrow CHBr_2OH + CH_2O + O_2 \tag{21b}$$
$$CHBr_2O_2 + CH_3O_2 \rightarrow CBr_2O + CH_3OH + O_2 \tag{21c}$$

Finally, the gas phase removal of CBr_2O, CHBrO, $CHBr_2O_2NO_2$, $CHBr_2O_2H$ and $CHBr_2OH$ are achieved via OH reaction, thermal decomposition and photolysis:

- for CBr_2O (Libuda et al. 1991) :

$$CBr_2O + h\nu \rightarrow CO + 2Br \tag{22}$$

- for CHBrO (Libuda et al. 1991) :

$$CHBrO + h\nu + O_2 \rightarrow CO + Br + HO_2 \tag{23}$$

- for $CHBr_2O_2NO_2$, by analogy with chlorinated compounds (Köppenkastrop and Zabel, 1991):

$$CHBr_2O_2NO_2 + M \rightarrow CHBr_2O_2 + NO_2 + M \tag{24}$$

and by analogy with $CH_3O_2NO_2$ (Atkinson et al., 2006):

$$CHBr_2O_2NO_2 + h\nu \rightarrow CHBr_2O_2 + NO_2 \tag{25a}$$
$$CHBr_2O_2NO_2 + h\nu \rightarrow CHBrO + Br + NO_3 \tag{25b}$$

- for $CHBr_2O_2H$, based on the reaction of CH_3O_2H (Atkinson et al., 2006):

$$CHBr_2O_2H + h\nu \rightarrow CHBrO + Br + OH \tag{26}$$
$$CHBr_2O_2H + OH \rightarrow CHBr_2O_2 + H_2O \tag{27}$$

- for $CHBr_2OH$:

$$CHBr_2OH + OH + O_2 \rightarrow CBr_2O + HO_2 + H_2O \tag{28}$$

The later reaction is assumed to proceed by the same mechanism as methanol (Atkinson et al., 2006).

All reactions and kinetic parameters are gathered in Table 4 and Fig. 1.

2.4. Dibromomethane degradation mechanism

For CH_2Br_2, reaction with OH is generally the major loss process (Ko and Poulet et al., 2003). The degradation of CH_2Br_2 is described in a similar way as for $CHBr_3$.

2.4.1. OH- or Cl-initiated oxidation of CH_2Br_2

The oxidation of CH_2Br_2 by OH or Cl leads to the H-abstraction to form $CHBr_2$ and after reaction with O_2, forms $CHBr_2O_2$:

$$CH_2Br_2 + OH + O_2 \rightarrow CHBr_2O_2 + H_2O \tag{29}$$

$$CH_2Br_2 + Cl + O_2 \rightarrow CHBr_2O_2 + HCl \tag{30}$$

The peroxy radical formed in this way is the same as from the $CHBr_3$ photolysis and its degradation kinetics and mechanism have thus been already described in the previous section. This degradation way of CH_2Br_2 is summarized in Table 5 and Fig. 1.

2.4.2. Photolysis of CH_2Br_2

The photolysis of CH_2Br_2 leads to the direct elimination of a Br atom and the formation of the peroxy radical CH_2BrO_2:

$$CH_2Br_2 + h\nu \rightarrow CH_2BrO_2 + Br \tag{31}$$

CH_2BrO_2 can react with NO to form CH_2BrO (Mc Givern et al., 2004; Wallington et al., 1997) and then CH_2O (Chen et al. 1995):

$$CH_2BrO_2 + NO \rightarrow CH_2BrO + NO_2 \tag{32}$$

$$CH_2BrO \rightarrow CH_2O + Br \tag{33}$$

The reaction of CH_2BrO_2 with NO_2 proceeds via:

$$CH_2BrO_2 + NO_2 + M \rightarrow CH_2BrO_2NO_2 + M \tag{34}$$

Also, the reaction between $CHBr_2O_2$ and HO_2 may have three pathways:

$$CH_2BrO_2 + HO_2 \rightarrow CH_2BrO_2H + O_2 \tag{35a}$$

$$CH_2BrO_2 + HO_2 \rightarrow CH_2O + HOBr + O_2 \tag{35b}$$

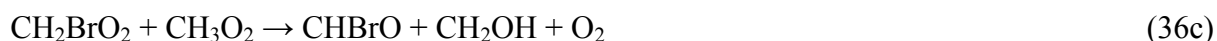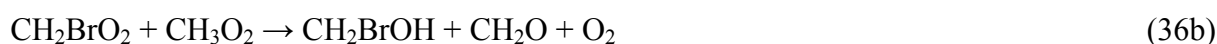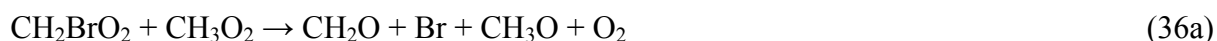$$CH_2BrO_2 + HO_2 \rightarrow CHBrO + H_2O + O_2 \tag{35c}$$

Mc Givern et al. (2004) considered pathways (a) and (b') only. Channel (b') gives as product CH_2BrO, OH and O_2 and then CH_2O and Br after CH_2BrO rapid decomposition.

As previously stated, the reaction enthalpies we calculated are in agreement with the theoretical data of Mc Givern et al. (2004) for brominated compounds, and of Hou et al.

(2005) for chlorinated compounds. We used the branching ratio of the analogous chlorine compounds, $k_{35a}/k_{35} = 0.2$ and $k_{35c}/k_{35} = 0.8$ (Catoire et al. 1996). However, experimental results of Chen et al. (1995) indirectly suggested the quasi exclusive CH_2BrO_2H formation, and another theoretical study for CH_2ClO_2 reaction (Wei and Zheng, 2007) reported that CH_2ClO_2H is the predominant product. Consequently, we also tested in another simulation the branching ratios, $k_{35a}/k_{35} = 0.9$ and $k_{35c}/k_{35} = 0.1$.

The reaction between CH_2BrO_2 and CH_3O_2 may occur via three channels. As previously stated, we have used the method proposed by Madronich et al. (1990) to estimate the branching ratio and found $k_{36a}/k_{36} = 0.7$, $k_{36b}/k_{36} = 0.3$ and $k_{36c}/k_{36} = 0$:

$$CH_2BrO_2 + CH_3O_2 \rightarrow CH_2O + Br + CH_3O + O_2 \tag{36a}$$

$$CH_2BrO_2 + CH_3O_2 \rightarrow CH_2BrOH + CH_2O + O_2 \tag{36b}$$

$$CH_2BrO_2 + CH_3O_2 \rightarrow CHBrO + CH_2OH + O_2 \tag{36c}$$

Then, $CH_2BrO_2NO_2$, CH_2BrO_2H, CHBrO and CH_2BrOH are transformed via OH reaction, thermal decomposition or photolysis:

- for CHBrO (Libuda et al. 1991):

$$CHBrO + h\nu + O_2 \rightarrow CO + Br + HO_2 \tag{37}$$

- for $CH_2BrO_2NO_2$, by analogy with chlorinated compounds (Köppenkastrop and Zabel, 1991):

$$CH_2BrO_2NO_2 + M \rightarrow CH_2BrO_2 + NO_2 + M \tag{38}$$

and by analogy with $CH_3O_2NO_2$ (Atkinson et al., 2006):

$$CH_2BrO_2NO_2 + h\nu \rightarrow CH_2BrO_2 + NO_2 \tag{39a}$$

$$CH_2BrO_2NO_2 + h\nu \rightarrow CH_2O + Br + NO_3 \tag{39b}$$

- for CH_2BrO_2H, based on the mechanism of CH_3O_2H (Atkinson et al., 2006):

$$CH_2BrO_2H + h\nu \rightarrow CH_2O + Br + OH \tag{40}$$

$$CH_2BrO_2H + OH \rightarrow CH_2BrO_2 + H_2O \tag{41}$$
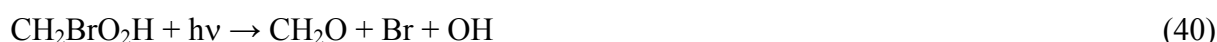
- for CH_2BrOH, based on the mechanism of $CH_3OH + OH$ (Atkinson et al., 2006):

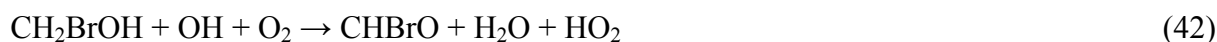$$CH_2BrOH + OH + O_2 \rightarrow CHBrO + H_2O + HO_2 \tag{42}$$

Table 5 and Fig. 1 summarize the overall degradation mechanism for CH_2Br_2 and the corresponding kinetic data. The choice of the kinetic data is detailed in Section 3.

3.   Description of the model used for the atmospheric simulations

The model used to study the degradation of bromoform and dibromomethane under atmospheric conditions is the meteorological/tracer transport model CATT-BRAMS (Coupled Aerosol Tracer Transport-Brazilian Regional Atmospheric Modeling system; Freitas et al. 2009) coupled on-line with the chemistry model described below. CATT-BRAMS is a 3D limited-area model, which is used here as a "pseudo" one dimensional model. For this, we run the model on a very small geographical domain and we set the initial conditions for the meteorological parameters horizontally uniform and vertically from a radiosounding corresponding to a stable atmosphere. These initial conditions are such that the atmosphere remains stable for the whole simulation duration. Stable atmospheric conditions are chosen to allow us studying the chemical degradation of bromoform and dibromomethane regardless of atmospheric perturbations such as convective transport and subsequent scavenging. A complementary study was conducted by Marécal et al. (2011) focusing on the impact on the local scale of tropical deep convection on the bromoform transport and chemical processing, including aqueous chemistry. Marécal et al. (2011) also used the CATT-BRAMS model with a fine horizontal resolution (1 km) allowing the cloud scale processes to be explicitly resolved (i.e. without convection parameterization).

In the present study, we use cyclic boundary conditions for the meteorological and chemical variables and a small geographical domain leading to 3D-chemical simulation fields quasi-uniform horizontally in the simulation, as checked *a posteriori*. With this setup, the model is not computationally costly. This allows us to run a large set of chemical reaction mechanism simulations to study in detail $CHBr_3$ and CH_2Br_2 degradations under realistic atmospheric conditions from surface to the upper troposphere.

The general setup common to all simulations is given hereafter. The specific characteristics of the different sensitivity simulations are given in Section 4.1. The model is set with 33 vertical levels spanning from the surface to 24 km altitude with layer depths increasing with altitude from 48 m near the surface to 1 km above 5.36 km height. The model is initialized vertically using the pressure, temperature and relative humidity data from the radiosounding launched from Darwin (Australia, 12°S–131°E) on 16 November 2005 at 2300UT in the frame of the SCOUT-O3 European Project (http://www.ozone-sec.ch.cam.ac.uk/scout o3/). We chose Darwin because it is located close to a warm ocean and coastal region where natural bromoform and dibromomethane emissions are expected to be strong (e.g. Quack and Wallace, 2003). The model starts on the radiosounding date and time. All simulations are performed for a time period of 10 days for $CHBr_3$ and 50 days for CH_2Br_2, corresponding to their estimated lifetime found in this region and season by our model.

Apart from $CHBr_3$ and CH_2Br_2 chemical degradation, a simple scheme including the chemical reaction mechanisms for CO, CH_4, total inorganic reactive nitrogen (NO_y) and hydrogen oxide radicals (HO_x) taken from Barth et al. (2007) has been used to simulate tropospheric chemistry. Chlorine chemistry has not been taken into account. Even if the reaction with Cl atom can be considered as loss mechanism for $CHBr_3$ and CH_2Br_2, reaction with OH remains the major loss mechanism. To avoid high increase of OH radicals in the lowest levels, dry deposition is applied to HNO_3 and O_3. The detailed bromine chemistry scheme implemented has been described in Section 2. We take into account 19 bromine-containing products deriving from the 2 SGs ($CHBr_3$, CH_2Br_2), including 14 organics PGs (CBr_3O_2, $CHBr_2O_2$, CH_2BrO_2, CBr_3O_2H, $CHBr_2O_2H$, CH_2BrO_2H, $CBr_3O_2NO_2$, $CHBr_2O_2NO_2$, $CH_2BrO_2NO_2$, CBr_2O, $CHBrO$, CBr_3OH, $CHBr_2OH$ and CH_2BrOH) and 5 inorganic PGs (Br, BrO, $BrONO_2$, HOBr and HBr).

For the initialization of the chemical species concentrations we have used outputs from the global Chemistry-Transport model (CTM) MOCAGE (Josse et al., 2004; Bousserez et al., 2007). They provide the background chemical conditions in which the degradation of bromoform and dibromethane are simulated. MOCAGE is based on the photochemical scheme RACM (Stockwell et al. 1997) for tropospheric chemistry and on REPROBUS (Lefèvre et al. 1994) for stratospheric chemistry. It includes a parameterization of convection representing subgrid scale transport and scavenging by deep convection. It also includes parameterizations for turbulent diffusion and dry deposition. We initialized CH_4, HNO_3, NO and NO_2, O_3 and CO mixing ratio by MOCAGE outputs from a specific simulation. The chosen horizontal resolution is a global $2°×2°$, with 47 vertical levels extending from the ground up to 5 hPa. Emissions correspond to those given by the former Intergovernmental Panel on Climate Change (IPCC) exercise, except for biogenic emissions which follow the inventory Global Emissions Inventory Activity (GEIA, http://www.geiacenter.org/). MOCAGE being a CTM, external meteorological forcings are necessary. In this simulation, 6-hourly analyses from ARPEGE Meteo-France's operational meteorological forecast model have been used. After a one-month spin-up, MOCAGE has been run for November 2005, and averaged over that month to provide initial conditions for the CATT-BRAMS model.

The present work reports modeling results for 2 scenarios (CLEAN and MODERATE), with tropospheric conditions ranging from clean to moderately polluted air masses. All simulations take place at the same latitude and longitude (12°S, 131°E). However, to initialize the simulation under realistic conditions of moderate pollution and clean atmosphere, we have used the MOCAGE model outputs for Darwin (12°S, 131°E) and for the

Pacific Ocean (5°N, 149°E), respectively. Initialization values at 1 km altitude for the 2 scenarios are given in Table 6. In addition, bromoform volume mixing ratio, as shown in Fig. 2, is initialized in two different ways: firstly by using the mean tropical data from ground to 19 km altitude (Fig. 2A) referenced by Montzka and Reimann et al. (2011) and secondly, by using the maximum values of the experimental data from Yokouchi et al. (2005) at ground along coasts of tropical islands in Pacific ocean (23.8 pptv for Kiribati, 1.9°N, 157°W) and the mean value of the observations from 10 km to 17 km altitude referenced by Montzka and Reimann et al. (2011) (Fig. 2B). Dibromomethane concentrations are initialized by the maximum values of the observations referenced by Montzka and Reimann et al. (2011) shown in Fig. 3. The missing data are interpolated from concentration profile observations (reported by Hossaini et al., 2010). The $CHBr_3$ and CH_2Br_2 degradations have been studied without other bromine sources during the simulations. Consequently, the total bromine during the simulations represents the bromine introduced at the beginning.

Most of the reaction rate constants used are from JPL (Sander et al., 2011), IUPAC (Aktinson et al., 2006), and MCM (Master Chemical Mechanism; Jenkin et al., 1997). Photolysis rates are computed on-line using Fast-TUV (Tie et al., 2003) consistently with the radiative calculations of the meteorological model (Toon et al., 1989). The kinetics parameters for the brominated VSLS degradation reactions are not well known. Consequently, we applied the rate constants of the reactions of analogous chlorine-containing species to the bromine reactions, when available. However, for the reactions $CHBr_2O_2$ + NO, CH_2BrO_2 + NO, CBr_3O_2 + OH, $CHBr_2O_2H$ + OH and CH_2BrO_2H + OH, the analogous chlorine rate constants are not known, and thus the generalized reactions RO_2 + NO and RO_2 + OH proposed by Jenkin et al. (1997) are used. All the rate constants associated with the reaction mechanisms described in Section 2 are gathered in Table 4 for $CHBr_3$ and in Table 5 for CH_2Br_2. The photolysis data of the reactions are from JPL 2011 (Sander et al., 2011), except for the brominated RO_2H and RO_2NO_2 for which the absorption cross sections of CH_3O_2H and $CH_3O_2NO_2$ have been used, respectively.

4. Modeling of the atmospheric degradation of $CHBr_3$ and CH_2Br_2: results and discussion

4.1. Chemical mechanism setup of the simulations

First, the 2 scenarios of clean and moderately polluted atmospheres (Table 6) have been tested in the reference simulation, including all the reactions for the 2 different initializations of bromoform (Fig. 2A and 2B). Then, the influences of the reaction RO_2 + NO_2 in simulation #1 and of the reaction RO_2 + CH_3O_2 in simulation #2 with respect to the reference simulation have been tested. In simulation #3, the influence of the branching ratio values in the cross reactions RO_2 + HO_2 has been analyzed by comparing the best current estimates with the values $k_{6a}/k_6 = k_{6b}/k_6 = 0.5$ for CBr_3O_2 + HO_2 and $k_{20a}/k_{20} = k_{20b}/k_{20} = 0.5$ for $CHBr_2O_2$ + HO_2 (Hossaini et al., 2010). All these sensitivity tests have been performed in clean atmosphere and for the bromoform initialization from Fig. 2B (maximum values). All the chemical mechanism setups are summarized in Table 7 for $CHBr_3$.

For dibromomethane degradation, both clean and moderately polluted atmosphere scenarios have been tested in the reference simulation (Table 8). A sensitivity test on the effect of the branching ratio for the CH_2BrO_2 + HO_2 reaction has been performed under clean atmospheric conditions (for reasons described in Section 4.3). Indeed, there is some uncertainty associated to them. The experimental results of Chen et al. (1995) and theoretical results of Wei and Zheng (2007) suggested the predominant formation of CH_2BrO_2H for the reaction between CH_2BrO_2 and HO_2, i.e. $k_{35a}/k_{35} = 1$. However, the branching ratios used in the reference simulation, by analogy to the chlorinated compound, were $k_{35a}/k_{35} = 0.2$ (formation of CH_2BrO_2H) and $k_{35c}/k_{35} = 0.8$ (formation of HCHO and H_2O).

In addition, the Henry's law constants for each intermediate degradation product derived in Section 2.2 have been explicitly taken into account for the interpretation of the results in each simulation. To assess the effect of the changes in the chemical scheme setup, the temporal evolution of each species is described and their solubility is discussed. The vertical profiles of each species are also discussed for altitudes below 6 km. The 6 km altitude corresponds to the maximum altitude for clouds containing liquid water in general. Indeed, the solubility regarding the Henry's law constant does not make sense at higher altitude where clouds are principally composed of ice. The results above 6 km are used only for the discussion of the lifetime of the species. Finally, for each case, the quantities of bromine potentially able to reach the TTL are discussed only in relation to the solubility of each species, which corresponds to the sum of the least soluble products, that is species with Henry's law constants lower than 10^4 mol L^{-1} atm^{-1} (the inorganics Br, BrO, HOBr, and the organics CBr_2O, CHBrO, and for dibromomethane degradation, CH_2BrOH and CH_2BrO_2H), as detailed in Section 2.2. However even if highly soluble, $BrONO_2$ is included in the

calculation of Br able to reach the TTL since this species undergoes hydrolysis in clouds and rain droplets, leading to the release of HOBr (Yang et al., 2005):

$$BrONO_2 + H_2O_{(aq)} \rightarrow HOBr + HNO_3 \tag{43}$$

HOBr has low solubility and may also reach the TTL.

HBr is not taken into account as potentially able to reach the TTL because it has a high acidity constant $K_a = 10^9$ leading to a high effective Henry's law constant as detailed in Section 2.2 (Yang et al., 2005).

4.2. CHBr₃ degradation

4.2.1. Influence of air pollution on the reference simulation

The influence of a moderate increase in the NO_y concentration (NO_x and HNO_3) on CHBr₃ degradation has been considered as indicated in Table 6. The overall lifetime of CHBr₃ depends on its reaction with OH and its photolysis. Fig. 4A and Fig. 4B show the lifetimes due to the reaction with OH (τ_{OH}) and the photolysis ($\tau_{photolysis}$) and the total lifetime τ_{total} of CHBr₃ deduced ($1/\tau_{total}=1/\tau_{photolysis} + 1/\tau_{OH}$) for the two atmospheric conditions, clean and polluted atmospheres. We observe the reduction of $\tau_{photolysis}$ and on the contrary, the increase of τ_{OH} with altitude because of the decrease of OH concentration (Fig. 5) and the increase of actinic flux with altitude. That means the contribution of the reaction with OH to the global lifetime decreases with the altitude and becomes quasi insignificant at 10 km altitude. So, the photolysis lifetime becomes quasi similar to the global lifetime τ_{total} at 10 km height (Fig. 4). The same trend is observed for both atmospheric conditions. However, the values of the lifetimes diverge, depending on the pollution conditions. The simulation shows that a moderate pollution leads to higher OH radical concentrations (due to the increase in O_3 production) at the lower altitude levels (< 10 km), as seen in Fig. 5 (for 10-days of OH average concentration). Therefore the CHBr₃ lifetime due to OH reaction is reduced in polluted atmosphere, as shown in Fig. 4. For instance the CHBr₃ lifetime due to OH at 5 km height decreases from 45.2 days in clean atmosphere to 31.8 days in a moderately polluted atmosphere, and consequently decreases the total lifetime at this altitude from 10.1 to 9.4 days. These lifetimes are lower than the local tropospheric lifetime of CHBr₃ of 26 days given by Ko and Poulet et al. (WMO, 2003) at 5 km. This is due to the higher OH concentration we used (4×10^6 molecule cm^{-3} compared to 1×10^6 molecule cm^{-3} in Ko and Poulet, 2003), and

to the stronger solar actinic flux used in our study, which takes place in November at low latitude (12.4°S).

Fig. 6 shows the vertical profiles of Br derived for the different species: $CHBr_3$, total organics, HBr and total inorganics except HBr, at 4 different dates (17 November 2005, i.e. 1 day after the beginning of the simulation, and 20, 23, 26 November 2005) and for the initializations used, as given in Fig. 2A. Fig. 6 (top panel) shows the decrease of Br contained in $CHBr_3$ from one day to another, more efficient in polluted atmosphere due to OH increase, as discussed above. Due to the $CHBr_3$ degradation, the concentration of Br from the organics (CBr_3O_2, $CHBr_2O_2$, CBr_2O, $CHBrO$, CBr_3O_2H, $CHBr_2O_2H$, $CBr_3O_2NO_2$, $CHBr_2O_2NO_2$, CBr_3OH or $CHBr_2OH$) increases and starts to decrease at the end of the simulation, i.e. between the 23 and 26 November (upper middle panel). In polluted atmosphere, the organics production and degradation are more efficient than in clean atmosphere, but follow approximately the same evolution as a function of time. Finally, due to the degradation of bromoform and organics, the production of inorganics as HBr, BrO, $BrONO_2$, HOBr and Br is observed (Fig. 6, lower middle and bottom panels). The production of HBr is more efficient in clean atmosphere, particularly at the end of the simulation. On the contrary, the other inorganics (BrO, $BrONO_2$, HOBr and Br) are produced most often in a polluted atmosphere with a maximum occurring at 1.5 km height. HBr is the final product of the PG degradation. It is formed by the reaction of bromine atom with HO_2 and HCHO. The time to reach this final state closely depends on the formation of the inorganic bromine atom reservoir HOBr and $BrONO_2$. In a clean atmosphere, HOBr production is more important compared to the production of $BrONO_2$. In the case of a more polluted atmosphere, inorganic bromine reservoir is principally composed of $BrONO_2$ because the reaction between BrO and NO_2, leading to the formation of $BrONO_2$, is more efficient than the reaction between BrO and HO_2. $BrONO_2$ lifetime (1.5 h) is larger than HOBr lifetime (15 min). Consequently, HBr is less rapidly produced in a polluted atmosphere than in a clean atmosphere. The rapid decrease at low altitude (below 1 km) and the rapid increase observed for all inorganic PGs (except HBr), which is more evident after the 20 November, is the consequence of the OH profile (Fig. 5). The OH profile is linked to the O_3 and HNO_3 profiles. In particular, the lower part of the OH profile is decreasing because of the dry deposition of O_3 and HNO_3. All these conclusions for initialization with the $CHBr_3$ profile shown in Fig 2A are identical when assuming the Fig. 2B initialization, i.e. the values of all the PGs increase in the same proportions. For all species, the profile trends are similar as a function of the degradation time

at all altitudes. In the following, the discussion focuses on the results at 1 km altitude, at which the maximum values of organics and inorganics are observed.

Fig. 7 shows the sum of the least soluble species (CBr_2O, $CHBrO$, $HOBr$, Br, BrO and $BrONO_2$) and the sum of the most soluble species (CBr_3O_2H, $CHBr_2O_2H$, CBr_3OH, $CHBr_2OH$ and HBr) for both scenarios (clean and polluted atmospheres) at 1 km height. Fig. 7A corresponds to the initial $CHBr_3$ mixing ratio of Fig. 2A, and Fig. 7B refers to the initial $CHBr_3$ mixing ratio of Fig. 2B. At the beginning of the simulation, the most soluble species and least soluble species are in comparable mixing ratios in the clean atmosphere. After three days of simulation, the most soluble species mixing ratios become more important and keep increasing in the clean atmosphere. On the contrary, during all the simulations in the polluted atmosphere, the least soluble species dominate. The concentration of the least soluble species increases and then becomes quasi stable after a few days of simulation for both scenarios.

Table 9 shows the relative partitioning of Br atom contained in each species after 10 days of simulation (the approximate lifetime of $CHBr_3$). Since mixing ratios of the least soluble species are quasi stable after a few days of simulation, the following results are available for this period. Around 48% (45.3 – 49.9%) of the total number of bromine atoms is in the form of inorganic species for both scenarios (clean and moderately polluted atmospheres) in the reference simulation. As shown previously, in the clean atmosphere the inorganic species dominate, mainly in the form of HBr (36% among 45.3%), which is essentially washed out. In the polluted atmosphere, the contribution of inorganic species ($HOBr$, Br, $BrONO_2$, BrO representing 26.4% among the 49.9% of total inorganic products) is similar to that of HBr (23.5%) and is mainly due to $BrONO_2$. $BrONO_2$ formed via the reaction between BrO and NO_2 is more abundant due to higher NO_2 concentrations in the moderately polluted atmosphere. After 10 days of simulation, for both scenarios around 18% (17.1-19.2%) of bromine is contained in the organics species. However, a detailed observation of these organic species shows that the temporal evolution of the least soluble species ($CHBrO$, CBr_2O, $CBr_3O_2NO_2$ and $CHBr_2O_2NO_2$) is different, compared to the most soluble species (CBr_3O_2H, $CHBr_2O_2H$, CBr_3OH and $CHBr_2OH$), depending on the scenario (clean or moderately polluted atmosphere). The production of the most soluble organic species given above decreases from 3.9% to 2.6% of the total bromine from clean to polluted atmosphere, because the cross reactions between peroxy radicals are more important in a clean atmosphere, as explained in Section 2. In contrast, the production of the least soluble species (mainly CBr_2O and $CHBrO$) increases from 13.2% to 16.6% of the total bromine from clean

to polluted atmospheres. Among these species, the production of $CBr_3O_2NO_2$ and $CHBr_2O_2NO_2$ is more important in a polluted atmosphere but remains negligible.

In summary, the production of the least soluble species such as CBr_2O and $CHBrO$ for organics and BrO, $HOBr$, $BrONO_2$ and Br for inorganics increases from 22.5% of the total bromine in clean atmosphere to 43% in moderately polluted atmosphere, as seen in Table 9.

4.2.2. Influence of the peroxy radicals reactions

Table 7 summarizes all the reactions of the peroxy radicals which have been taken into account in the simulations. The impact of the $RO_2 + NO_2$ reactions has been studied in simulation #1, where these reactions were removed compared to the reference simulation where they were included. The importance of these reactions depends on the NO_x level. For high NO_x level, the reactions between RO_2 and NO_2 may enter in competition with the reactions between RO_2 and NO. Under our conditions of NO_x level (0.036 ppbv and 0.061 ppbv), there is no effect on $CHBr_3$ degradation because the production of RO_2NO_2 species are negligible (Table 9).

The $RO_2 + CH_3O_2$ reactions have also been considered in our reference simulation and compared when removed in simulation #2. The production of the organic and inorganic products differs between simulations. The implementation of the $RO_2 + CH_3O_2$ reactions (reference simulation) decreases the production yields of CBr_3O_2H and $CHBr_2O_2H$ formed in $RO_2 + HO_2$ reactions, as shown in Table 9. The different peroxy radical reactions are indeed in competition, depending on their relative rates. The rate constant values of the reactions between CBr_3O_2 and CH_3O_2 (reaction (7)) and between CBr_3O_2 and HO_2 (reaction (6)) are 6.6 $\times 10^{-12}$ and 5.1×10^{-12} cm^3 molecule^{-1} s^{-1} at 298K, respectively. The rate constant values of the reactions between $CHBr_2O_2$ and CH_3O_2 (reaction (20)) and between $CHBr_2O_2$ and HO_2 (reaction (21)) are 1.2×10^{-12} and 5.9×10^{-12} cm^3 molecule^{-1} s^{-1} at 298 K, respectively. Considering the average during 10 days simulation volume mixing ratios of HO_2 (10.9 ppt) and CH_3O_2 (1.8 ppt) derived from the simulations, the $RO_2 + CH_3O_2$ reaction is thus around 5 times (for $RO_2 = CBr_3O_2$) to 30 times (for $RO_2 = CHBr_2O_2$) slower than the $RO_2 + HO_2$ reaction. Nevertheless, its occurrence leads to a decrease of the ($RO_2 + HO_2$) product yields, CBr_3O_2H and $CHBr_2O_2H$. To conclude on the effect of the $RO_2 + CH_3O_2$ reaction on $CHBr_3$ degradation mechanism, bromine mixing ratio potentially able to reach the TTL decreases from 23.7% of the total bromine (10.3 pptv) (simulation #2) to 22.5% of the total bromine (9.3 pptv) (reference simulation) for clean atmosphere, as seen in Table 9. Indeed, the soluble

species CBr_3OH (formed in reaction (7b)) and HBr are produced in more abundant quantities in the reference simulation, whereas the least soluble species CBr_2O and $BrONO_2$ are produced more often in simulation #2.

We have also investigated the difference between the present chemical scheme and that proposed by Hossaini et al. (2010) in simulation #3 for the clean atmosphere, in which the cross reactions ($RO_2 + HO_2$ and $RO_2 + CH_3O_2$) are more important since the NO_x level is lower (Table 6). The difference between simulation #3 and simulation #2 is only in the branching ratios for the reaction between RO_2 and HO_2 (reactions (6) and (20)). In simulation #2 and the reference simulation, reaction between CBr_3O_2 and HO_2 produces exclusively CBr_3O_2H (6a), and reaction between $CHBr_2O_2$ and HO_2 produces 70% $CHBr_2O_2H$ (20a) and 30% CBr_2O (20c). In simulation #3, reaction (6) produces 50% CBr_3O_2H (6a) and 50% CBr_2O (6b), and reaction (20) produces 50% $CHBr_2O_2H$ (20a) and 50% $CHBrO$ (20b). Table 9 shows that these branching ratio modifications for simulation #3 reduce the productions of CBr_2O (from 12.8% to 9.6%), CBr_3O_2H (from 1.0% to 0.6%) and $CHBr_2O_2H$ (from 1% to 0.8%) but raise the production of $CHBrO$ (from 1.5% to 1.9%), as organics products. By inspecting the chemical scheme more precisely (Fig. 1), we can notice that for simulation #2 or the reference simulation, the 100% CBr_3O_2H produced by pathway (6a) subsequently decomposes in CBr_2O and Br, whereas for simulation #3, the 50% CBr_3O_2H produced by pathway (6a) gives CBr_2O in the same amount, and 50% CBr_2O are produced by pathway (6b). Consequently, the production of CBr_3O_2H decreases in simulation #3 to 0.6%. Similarly, in simulation #2, the reaction between $CHBr_2O_2$ and HO_2 produces CBr_2O and principally $CHBr_2O_2H$ and then $CHBrO$, whereas in simulation #3, the same reaction produces as much $CHBr_2O_2H$ (and then $CHBrO$) as $CHBrO$ instead of CBr_2O in the simulation #2. Consequently, the production of $CHBr_2O_2H$ decreases in simulation #3 compared to simulation #2. Globally, the production of CBr_2O decreases and the production of $CHBrO$ increases in simulation #3. About the inorganic products, some changes are observable between the two simulations: simulation #3 results in an increase of these products to 46.1% with respect to 42.9% (#2), as shown in Table 9. Consequently, the change in the branching ratios in the reaction between RO_2 and HO_2 decreases the bromine concentration that could reach the TTL from 23.7% of the total bromine (10.3 pptv) (simulation #2) to 21.5% (8.8 pptv) (#3) mainly because the soluble species HBr is more produced in the simulation #3 and the less soluble species CBr_2O is more produced in simulation #2.

The differences between the reference simulation and simulation #3 are the addition of the $RO_2 + CH_3O_2$ (and the negligible $RO_2 + NO_2$) reaction in the reference simulation and the

changes in the branching ratio of the reactions between RO_2 and HO_2. The changes in simulation #3 reduce mainly the production of organic products (from 17.1% the reference to 12.9% for simulation #3), mainly in the form of the highly insoluble species CBr_2O and consequently reduce the total bromine that could reach the TTL from 22.5% (9.3 ppt) for the reference simulation to 21.5% (8.8 ppt) for simulation #3.

To conclude, as seen in Table 9, changes in the cross reactions have weak influences on the distribution of the organic and inorganic products. The bromine volume mixing ratio that could reach the TTL is around 22.5% of the total initial bromine.

These sensitivity tests permit the establishment of a simplified chemistry scheme for bromoform degradation. The reaction between RO_2 and NO_2 is not taken into account because it produces negligible mixing ratios of RO_2NO_2. Only pathways (a) and (c) are considered for the reaction between RO_2 and HO_2 and the reaction between $CHBr_2O_2$ and CH_3O_2 can be neglected because the product ratios from this reaction are 0 to 0.2% of the total bromine. The simplified chemical scheme is shown in Fig. 8. However, even if the previous tests on the degradation scheme have shown weak influence, the production of organic products remains important. The simplification of the $CHBr_3$ degradation scheme by the direct production of 3 Br atoms leads to underestimate the bromine potentially able to reach the TTL by 20% to 50%, depending on the NO_y atmospheric pollution.

4.3. CH_2Br_2 degradation

The influence of a moderate increase in the NO_y concentration (NO_x and HNO_3) on CH_2Br_2 degradation in the reference simulation has been tested. Then, some changes in the branching ratios in the reaction between CH_2BrO_2 and HO_2 have been tested in simulation #1.

According to Montzka and Reimann et al. (2011), CH_2Br_2 has a total lifetime longer than $CHBr_3$. The change in the atmospheric conditions from a clean to a polluted atmosphere increases the OH concentration and significantly influences the global lifetime of CH_2Br_2, decreasing from 72 days in a clean atmosphere to 53 days in a polluted atmosphere at 5 km height. Again, the higher CH_2Br_2 tropospheric lifetime of 120 days given by Ko and Poulet et al. (WMO, 2003) at 5 km height is due to the lower OH concentration used for their calculations (1×10^6 molecules cm^{-3}) and to the stronger solar actinic flux used in our study, which takes place in November at low latitude (12.4°S).

Fig. 9 shows the time evolution (during 50 days from 17 November to 5 January) of the vertical profiles of Br contained in several species. Br mixing ratio from CH_2Br_2 decreases

with time (top panel), less rapidly at the end of the simulation due to the decrease in the OH concentration. Br mixing ratio from organics increases during the first four days of the simulation and then decreases to form inorganics species. HBr is formed as a major product and keeps increasing during the simulation until the 20 December and then start decreasing. The other inorganic species increase and then become stable. CH_2Br_2 mixing ratio decreases more rapidly in the moderately polluted atmosphere (Fig. 9B). The production of organics species is more efficient in the moderately polluted atmosphere at the beginning of the simulation. The production of HBr is also more efficient in moderately polluted atmosphere. HBr is the final product of the PG degradation and the CH_2Br_2 degradation is more rapid in the moderately polluted atmosphere. The difference in lifetime between the polluted atmosphere and the clean atmosphere is more pronounced for CH_2Br_2 degradation (by 20 days) than for $CHBr_3$ degradation (by 1 day). Consequently, the more rapid degradation of CH_2Br_2 in the polluted atmosphere produces more rapidly the other inorganic species and then HBr, compared to the $CHBr_3$ degradation. Finally, the inorganic species mixing ratios are more important in the polluted atmosphere. As for $CHBr_3$, the results are only discussed at 1 km altitude.

Fig. 10 shows the sum of the least soluble species (CBr_2O, $CHBrO$, CH_2BrO_2H, CH_2BrOH, HOBr, Br, BrO and $BrONO_2$) and the sum of the most soluble species ($CHBr_2O_2H$, $CHBr_2OH$ and HBr) for both scenarios (clean and polluted atmosphere) at 1 km height. At the beginning of the simulation, the most soluble and least soluble species have comparable mixing ratios in the clean atmosphere. After 3 days of simulation, the soluble species become more important and keep increasing, and the least soluble species become quasi stable in clean atmosphere. On the contrary, during 21 days of simulation in the polluted atmosphere, the least soluble species dominate and then the soluble species become more important and keep increasing.

As for $CHBr_3$, the total bromine produced from CH_2Br_2 degradation that could reach the TTL has been calculated from the least soluble species (CBr_2O, $CHBrO$, Br, BrO, $BrONO_2$ and HOBr), resulting in an important increase of the total bromine, from 8.8% (0.19 pptv) in the clean atmosphere to 20.2% (0.42 pptv) in a moderately polluted atmosphere. The latter value is mainly due to the more efficient degradation of CH_2Br_2 giving principally inorganic products, including species other than HBr, with low solubility, as seen in Fig. 10 and Table 10.

Modification in the branching ratios for the reaction between CH_2BrO_2 and HO_2 has also been tested in simulation #1. The experimental results of Chen et al. (1995) are tested,

with $k_{35a}/k_{35} = 0.9$ (formation of CH_2BrO_2H) and $k_{35c}/k_{35} = 0.1$ (formation of HCHO and H_2O). Significant changes in the degradation products are not observable when the branching ratios are changed since all the species produced by the photolysis of CH_2Br_2 (leading to CH_2BrO_2) are totally negligible.

The atmospheric degradation scheme of CH_2Br_2 can be simplified. The photolysis pathway can be neglected and the OH or Cl pathway to form $CHBr_2O_2$ is similar to the $CHBr_3$ photolysis pathway, leading to the degradation mechanism from Fig. 8.

5. Conclusions

Detailed atmospheric degradation schemes for bromoform ($CHBr_3$) and dibromomethane (CH_2Br_2) have been established and implemented into a pseudo 1D model including the atmospheric chemistry of CH_4, CO, HO_x, NO_x, NO_y and O_x.

To help to set up the degradation schemes, standard reaction enthalpies at 298 K for the different pathways of the peroxy radical (RO_2 with R = CH_2Br, $CHBr_2$ or CBr_3) reactions with HO_2 have been calculated using quantum chemistry tools. These calculations, combined with previous results, have helped to estimate the relative importance of the different pathways. Brominated methyl hydroperoxides (RO_2H) are suggested to be the main products of these reactions.

Two empirical methods have been used to estimate the brominated organics Henry's law constants. The results show that the least soluble organic species resulting from the VSLS degradations are CBr_2O, $CHBrO$ (and negligible $CBr_3O_2NO_2$ and $CHBr_2O_2NO_2$, and negligible CH_2BrO_2H, CH_2BrOH and $CH_2BrO_2NO_2$ for CH_2Br_2 degradation). The potential ability of the product gases (PGs) to be transported in the TTL in regard to their solubility in case of deep convection has been computed in the 1D model under high sunlight conditions. The least soluble PGs can contribute to bromine in the stratosphere additionally to the original substances.

$CHBr_3$ and CH_2Br_2 concentrations have been initialized at the beginning of the simulations and then the degradation of these species has been studied without other bromine sources during the simulations. Consequently, the total bromine during the simulations represents the bromine introduced at the beginning. The full degradation scheme of $CHBr_3$ and CH_2Br_2 has been performed for two well defined scenarios of a clean and moderately

polluted atmosphere, as representative of a tropical coastal region where natural bromoform and dibromomethane emissions are expected to be important. For $CHBr_3$ degradation in a clean atmosphere, it is shown that approximately 22% of the total initial bromine is transformed into low solubility inorganic (Br, BrO, HOBr, $BrONO_2$: 9%) and organic (CBr_2O, CHBrO: 13%) species, and thus able to reach the TTL. A moderate rise in pollution (increase of NO_x by a factor of 2 and HNO_3 by a factor of 3) has been tested. When this type of pollution is considered, the total bromine potentially able to reach the TTL increases to 43% (26% of inorganics and 17% of organics).

According to the simulations the reactions between RO_2 and NO_2 have no effect on the bromoform degradation in clean and moderately polluted atmospheres. The importance of $RO_2 + CH_3O_2$ reactions has been tested in one sensitivity study in a clean atmosphere. It has a negligible effect on bromoform degradation, with the production of more soluble species and consequently a decrease in the amount of bromine potentially able to reach the TTL from 23.7% (without the CH_3O_2 reaction) to 22.5% (with the CH_3O_2 reaction).

Modifications in the branching ratios for the reaction between RO_2 and HO_2 have also been tested in a clean atmosphere. 100% for the CBr_3O_2H formation ($k_{6a}/k_6 = 1$) in the case of $CBr_3O_2 + HO_2$ reaction, and 70% for the $CHBr_2O_2H$ formation ($k_{20a}/k_{20} = 0.7$) and 30% for the CBr_2O formation ($k_{20c}/k_{20} = 0.3$) in the case of the $CHBr_2O_2 + HO_2$ reaction have been used as they are the best current estimates. These branching ratios are used instead of the values used until now, $k_{6a}/k_6 = 0.27$ or 0.5, $k_{6b}/k_6 = 0.73$ or 0.5, and $k_{20a}/k_{20} = 0.59$ or 0.5, $k_{20b}/k_{20} = 0.41$ or 0.5 (Mc Givern et al., 2004; Hossaini et al., 2010). This results in a small impact for the total bromine originating from $CHBr_3$ potentially able to reach the TTL: 23.7% in our simulation, instead of 21.5% for the previous used branching ratio values, as shown in Table 9.

The full CH_2Br_2 degradation scheme has been tested in a clean atmosphere and shows that approximately 8.8% (1.3% of organics and 7.5% of inorganics) of the total bromine potentially is able to reach the TTL. As observed for $CHBr_3$ degradation, a pollution rise induces the production of less soluble species and consequently increases significantly the Br quantity that could reach the TTL to 20.2 % (1.3% of organics and 18.9% of inorganics).

From this study, degradation schemes for bromoform and dibromomethane have been derived for modeling clean and moderately polluted atmospheres, as shown in Fig. 8. According to the simulations, dibromomethane degradation by photolysis is considered insignificant. The reactions between peroxy radicals and NO_2 produce species with negligible mixing ratios and have been removed in the final chemical scheme. Thus, only the pathways

of the reactions for RO_2 with HO_2, NO and CH_3O_2 are considered. Moreover, the formation of $CHBr_2OH$ and $CHBrO$ from the reaction between $CHBr_2O_2$ and CH_3O_2 appeared to be negligible (< 0.2% production) and has been removed in the final scheme. Finally, in contrast to $CHBr_3$, the production of organics species from CH_2Br_2 degradation could be neglected and the degradation scheme could also be reduced to the simple reaction CH_2Br_2 + OH or Cl $\rightarrow$ 2 Br.

In this paper we do not study the effect of more polluted urban atmosphere on bromoform and dibromomethane degradations and in particular, the importance of the reaction between RO_2 and NO_2 when the level of NO_x is very high. More complex chemistry (including volatile organic compounds) should be integrated to the modeling system in order to simulate an urban atmosphere in the vicinity of the tropical western Pacific, like the Singapore atmosphere.

Acknowledgments

References

Aschmann J., Sinnhuber B.-M., Atlas E. L., and Schauffler S. M., 2009. Modeling the transport of very short-lived substances into the tropical upper troposphere and lower stratosphere, Atmos. Chem. Phys., 9, 9237-9247, doi:10.5194/acp-9-9237-2009.

Atkinson R., Baulch D.L., Cox R.A., Crowley J.N., Hampson, R.F., Hynes R.G., Jenkin M.E., Rossi M.J., Troe J., 2006. Evaluated kinetic and photochemical data for atmospheric

chemistry: Volume II – gas phase reactions of organic species. Atmospheric Chemistry and Physics 6, 3625 – 4055.

Barth M.C., Kim S-W., Skamarock W.C., Stuart A.L., Pickering K.E., Ott L.E., 2007. Simulations of the redistribution of formaldehyde, formic acid, and peroxides in the July 1996 stratospheric-tropospheric experiment: radiation, aerosols and ozone deep convection storm. Journal of Geophysical Research 112 (D13310). doi:10.1029/2006JD008046.

Bousserez N., Attié J.-L., Peuch V.-H., Michou M., Pfister G., Edwards D., Avery M., Sachse G., Browell E., Ferrare E., 2007. Evaluation of MOCAGE chemistry and transport model during the ICARTT/ITOP experiment, Journal of Geophysical Research 112 (D120S42), doi:10.1029/2006JD007595.

Brioude J., Portmann R. W., Daniel J. S., Cooper O. R., Frost G. J., Rosenlof K. H., Granier C., Ravishankara A. R., Montkza S. A., and Sthol A., 2010.Variations in ozone depletion potentials of very short-lived substances with season and emission region, Geophys. Res. Lett., 37, L19804, doi:10.1029/2010GL044856.

Caralp F., Lesclaux R., Rayez M.-T., Rayez J.-C., Forst W., 1988. Kinetics of the Combination Reactions of Chlorofluoromethylperoxy Radicals with NO, in the Temperature Range 233-373 K. Journal of the Chemical Society - Faraday Transaction II 84, 569 – 585.

Catoire V., Lesclaux R., Lightfoot P. D., Rayez M.-T., 1994. Kinetic Study of the Reactions of CH_2ClO_2 with Itself and with HO_2, and Theoretical Study of the Reactions of CH_2ClO, between 251 and 600 K. Journal of Physical Chemistry 98, 2889 – 2898.

Catoire V., Lesclaux R., Schneider W.F., Wallington T.J., 1996. Kinetics and Mechanisms of the Self-Reactions of CCl_3O_2 and $CHCl_2O_2$ Radicals and Their Reactions with HO_2. Journal of Physical Chemistry 100, 14356 – 14371.

Chen J., Catoire V., Niki H., 1995. Mechanistic study of $BrCH_2O$ radical degradation in 700 Torr air. Chemical Physics Letters 245, 519 – 528.

Čížek J., 1969. In: Hariharan P.C. (Ed.), Advances in Chemical Physics, Wiley Interscience, New York, 14, pp.35.

Dognon A.M., Caralp F., Lesclaux R., 1985. Réactions des radicaux chlorofluorométhyl peroxyles avec NO: Etude cinetique dans le domaine de température compris entre 230 et 430 K. Journal de chimie physique et de physico-chimie biologique 82, 349–352.

Dorf M., Butz A., Camy-Peyret C., Chipperfield M.P., Kritten L., Pfeilsticker K., 2008. Bromine in the tropical troposphere and stratosphere as derived from ballon-borne BrO observations, Atmospheric Chemistry and Physics 8, 7265–7271.

Dunning Jr T.H., 1989. Gaussian basis sets for use in correlated molecular calculations. I. The atoms boron through neon and hydrogen. Journal of Chemical Physics 90, 1007–1024.

Freitas S. R., Longo K. M., Silva Dias M. A. F., Chatfield R., Silva Dias P., Artaxo P., Andreae M. O., Grell G., Rodrigues L. F., Fazenda A., Panetta J., 2009. The Coupled Aerosol and Tracer Transport model to the Brazilian developments of the Regional Atmospheric Modeling System (CATT-BRAMS). Part 1: model description and evaluation, Atmospheric Chemistry and Physics 9, 2843–2861.

Frisch M.J., Trucks G.W., Schlegel H.B., Scuseria G.E., Robb M.A., Cheeseman J.R., Montgomery Jr. J.A., Vreven T., Kudin K.N., Burant J.C., et al., 2004. Gaussian 03, Revision D.01. Gaussian, Inc., Wallingford, CT.

Frisch M.J., Trucks G.W., Schlegel H.B., Scuseria G.E., Robb M.A., Cheeseman J.R., Scalmani G., Barone V., Mennucci B., Petersson G.A., et al., 2009. Gaussian 09, Revision A.02. Gaussian, Inc., Wallingford CT.

Goodson D.Z. 2002. Extrapolating the coupled-cluster sequence toward the full configuration-interaction limit. Journal of Chemical Physics, 116, 6948-6956.

Henon E., Bohr, F., Canneaux S., Postat B., Auge F., Bouillard E., Domureau V., 2003. KISTHEP version 1.0: a Kinetic and Statistical Thermodynamical Package. University of Reims Champagne-Ardenne, France, available on request to the authors of the present paper.

Hense I., Quack B., 2009. Modelling the vertical distribution of bromoform in the upper water column of the tropical Atlantic Ocean. Biogeosciences, 6, 535–544.

Hossaini R., Chipperfield M.P., Monge-Sanz B.M., Richards N.A.D., Atlas E., and Blake D. R., 2010. Bromoform and dibromethane in the tropics: a 3-D model study of chemistry and transport, Atmospheric Chemistry and Physics 10, 719–735.

Hou H., Deng L., Li J., Wang B., 2005. A Systematic Computational Study of the Reactions of HO_2 with RO_2: The HO_2 + CH_2ClO_2, $CHCl_2O_2$, and CCl_3O_2 Reactions. Journal of Physical Chemistry A 109, 9299–9309.

Jenkin M.E., Saunders S.M., Pilling M.J., 1997. The tropospheric degradation of volatile organic compounds: A protocol for mechanism development. Atmospheric environment 31, 81–104.

Johnson R.D., 2011: NIST Computational Chemistry Comparison and Benchmark Database. R.D. Johnson, III (Ed.). NIST Standard Reference Database Number 101 Release 15b.

Josse B., Simon P., Peuch V.H., 2004. Radon global simulations with the multiscale chemistry and transport model MOCAGE. Tellus B 56, 339–356.

Kambanis K. G., Lazarou Y. G., Papagiannakopoulos P. J., 1997. Absolute Rate Constants for the Reactions of Cl Atoms with CH_3Br, CH_2Br_2, and $CHBr_3$. J. Phys. Chem., 101, 8496-8502.

Kamboures M.A., Hansen J.C., Francisco J.S., 2002. A study of the kinetics and mechanism involved in the atmospheric degradation of bromoform by atomic chlorine. Chemical Physics Letters, 353, 335–344.

Kendall R.A., Dunning Jr. T.H., Harrison R.J., 1992. Electron affinities of the first-row atoms revisited. Systematic basis sets and wave functions. Journal of Chemical Physics 96, 6796–6807.

Kerkweg A., Jöckel P., Warwick N., Gebhardt S., Brenninkmeijer C. A. M., Lelieveld J., 2008. Consistent simulation of bromine chemistry from the marine boundary layer to the stratosphere – Part 2: Bromocarbons. Atmospheric Chemistry and Physics 8, 5919–5939.

Ko M.K.W, Poulet G. (leads authors) et al., 2003. Very Short-Lived Halogen and Sulfur Substances. Chapter 2 in Scientific Assessment of Ozone Depletion: 2002, Global Ozone Research and Monitoring Project—Report No. 47, World Meteorological Organization, Geneva.

Köppenkastrop D., Zabel F., 1991. Thermal decomposition of chlorofluoromethyl peroxynitrates. International Journal of Chemical Kinetics 23, 1.

Kirchner F., Mayer-Figge A., Zabel F., Becker K.H., 1998. Thermal Stability of Peroxynitrates. International Journal of Chemical Kinetics 31, 127–144.

Law K.S., Sturges W.T. (leads authors) et al., 2007. Halogenated Very Short-Lived Substances Chapter 2 in Scientific Assessment of Ozone Depletion: 2006, Global Ozone Research and Monitoring Project—Report No. 50, WorldMeteorological Organization, Geneva, Switzerland, pp. 572.

Lesclaux R., 1997. Combination of peroxyl radicals in the gas-phase. In: Alfassi, Z.B. (Eds.), Peroxyl Radicals, Wiley, New York, pp. 81–112.

Lefèvre F., Brasseur G. P., Folkins I ., Smith A . K., and Simon P., 1994. Chemistry of the 1991-1992 stratospheric winter: Three-dimensional model simulations. Journal of Geophysical Research ,99, NO. D4, 8183-8195.

Libuda H. G., Zabel F., Becker K. H., 1991. UV spectra of some organic chlorine and bromine compounds of atmospheric interest. Kinetics and Mechanisms for the Reactions of Halogenated Organic Compounds in the Troposphere. STEP-HALOCSIDE/AFEAS WORKSHOP, Dublin, Ireland.

Madronich S., Calvert J.G., 1990. Permutation Reactions of Organic Peroxy Radicals in the Troposphere. Journal of Geophysical Research 95, 5697–5715.

Marécal V., Pirre M., Krysztofiak G., Josse B. 2011. What do we learn on bromoform transport and chemistry in deep convection from fine scale modelling? Atmos. Chem. Phys. Discuss., 11, 29561–29600.

Maricq M. M., Shi J., Szente J. J., Rimai L., Kaiser E. W., 1993. Evidence for the three-center elimination of hydrogen chloride from 1-chloroethoxy. Journal of Physical Chemistry 97, 9686.

McGivern W. S., Kim H., Francisco, J. S. and North S. W., 2002. Investigation of the Atmospheric Oxidation Pathways of Bromoform: Initiation via OH/Cl reactions. Journal of Physical chemistry A, 106, 6395-6400.

McGivern W. S., Kim H., Francisco, J. S. and North S. W., 2004. Investigation of the Atmospheric Oxidation Pathways of Bromoform and Dibromomethane: Initiation via UV Photolysis and Hydrogen Abstraction. Journal of Physical chemistry A, 108, 7247-7252.

Meylan W.M., Howard P.H., 1991. Bond contribution method for estimating Henry's law constants. Environmental Toxicology and chemistry 10, 1283–1293.

Møller C., Plesset M.S., 1934. Note on an Approximation Treatment for Many-Electron Systems. Physical Review 46, 618–622.

Montzka S. A., Reimann S. (lead authors) et al., 2011. Ozone-Depleting Substances (ODSs) and Related Chemicals. Chapter 1 in Scientific Assessment of Ozone Depletion: 2010, Global Ozone Research and Monitoring Project—Report No. 52, World Meteorological Organization, Geneva.

Niki H., Maker P. D., Savage C. M., Breitenbach L. P., 1980. FTIR studies of the kinetics and mechanism for the reaction of Cl atom with formylchloride. International Journal of Chemical Kinetics 12, 915–920.

Nirmalakhandan N. N., Speece R.E., 1988. Prediction of Aqueous Solubility of Organic Chemicals Based on Molecular Structure. Environmental Science and Technology 22, 328–338.

Orlando J.J., Tyndall G.S., Wallington T.J., 1996. Atmospheric Oxidation of CH3Br: Chemistry of the CH_2BrO Radical. Journal of Physical Chemistry 100, 7026–7033.

Peterson K.A., Woon D.E., Dunning Jr. T.H., 1994. Benchmark calculations with correlated molecular wave functions. IV. The classical barrier height of the H+H$_2$→H$_2$+H reaction. Journal of Chemical Physics 100, 7410–7416.

Pisso I., Haynes P. and law K. S., 2010. Emission location dependent ozone depletion potentials for very short-lived halogenated species, Atmos. Chem. Phys., 10, 12025-12036.

Pople J.A., Head-Gordon M., Raghavachari K., 1987: Quadratic configuration interaction. A general technique for determining electron correlation energies. Journal of Chemical Physics 87 5968–5976.

Purvis III G.D., Bartlett R.J., 1982. A full coupled-cluster singles and doubles model: The inclusion of disconnected triples J. Chem. Phys., 76, 1910.

Quack B., and Wallace D. W. R., 2003. Air-sea flux of bromoform: Controls, rates, and implications, Global Biogeochem. Cycles, 17(1), 1023, doi:10.1029/2002GB001890.

Sander R., 1999. Compilation of Henry's Law Constants for Inorganic and Organic Species of Potential Importance in Environmental Chemistry (Version 3) http://www.henrys-law.org.

Sander S. P., Friedl R.P., Abbatt J.P.D., Barker J.R., Burkholder J.B., Golden D. M., Kolb C. E., Kurylo M. J., Moortgat G. K., Wine P. H., Huie R. E., Orkin V.L., 2011. Chemical Kinetics and Photochemical Data for Use in Atmospheric Studies Evaluation Number 17. JPL Publication 10-6.

Scuseria G.E., Janssen C.L., Schaefer III, H.F., 1988. An efficient reformulation of the closed-shell coupled cluster single and double excitation (CCSD) equations. Journal of Chemical Physics 89 7382–7386.

Scuseria G.E., Schaefer III, H.F., 1989. Is coupled cluster singles and doubles (CCSD) more computationally intensive than quadratic configuration interaction (QCISD)? Journal of Chemical Physics 90 3700–3704.

Seinfeld J.H., Pandis S.N. 2006. Atmospheric chemistry and physics: from Air Pollution to Climate Change, chapter 7, Second edition, John Wiley & Sons Ed, Inc., New York.

Shallcross D.E., Raventos-Duran M. T., Bardwell M.W., Bacak A., Solman Z., Percival C. J., 2005. A semi-empirical correlation for the rate coefficients for cross- and self-reactions of peroxy radicals in the gas-phase. Atmospheric Environment 39, 763–771.

Sinnhuber B.-M., Rosanov A., Sheode N., Afe O. T., Richter A., Sinnhuber M., Wottrock F., Burrows J. P., Stiller G. P., von Clarmann T., Linden A., 2005. Global observations of

stratospheric bromine monoxide from SCIAMACHY, Geophysical Research and Letters 32 (L20810). doi :10.1029/2005GL023829.

Stockwell W.R., Kirchner F., Kuhn M., Seefeld S., 1997. A New Mechanism for Regional Atmospheric Chemistry Modeling. Journal of Geophysical Research 102, 25847–25879.

Tie, X., Madronich, S., Walters, S., Zhang, R., Rasch, P., and Collins, W., 2003. Effects of clouds on photolysis and oxidants in the troposphere. Journal of Geophysical Research, 108, 4642,doi:10.1029/2003JD003659.

Toon O.B., McKay C.P., Ackerman T.P., Santhanam K.L., 1989. Rapid calculation of radiative heating rates and photodissociations rates in inhomogeneous multiple scattering atmospheres. Journal of Geophysical Research 94, 16287–16301.

Tuazon E.C, Atkinson R., 1994. Tropospheric Reaction Products and Mechanisms of the Hydrochlorofluorocarbons 141b, 142b, 225ca, and 225cb. Environmental Science and Technology 28, 2306–2313.

Tyndall G. S., Wallington T. J., Ball J. C., 1998. FTIR Product Study of the Reactions CH_3O_2 + CH_3O_2 and CH_3O_2 + O_3. Journal of Physical Chemistry A 102, 2547–2554.

Tyndall G.S., Cox R.A., Granier C., Lesclaux R., Moortgat G.K., Pilling M.J., Ravishankara A.R., Wallington T.J., 2001. Atmospheric chemistry of small organic peroxy radicals. Journal of Geophysical Research 106, 12157–12182.

Vaghjiani G. L., Ravishankara A. R., 1989. Absorption Cross Sections of CH_3O_2H, H_2O_2, and D_2O_2 Vapours between 210 and 365 nm at 297 K. Journal of Geophysical Research 94, 3487–3492.

Villenave E., Lesclaux R., 1996. Kinetics of the Cross Reactions of CH_3O_2 and $C_2H_5O_2$ Radicals with Selected Peroxy Radicals. Journal of Physical Chemistry 100, 14372–14382.

Wallington T.J., Dagaut P., Kurylo M.J., 1992. Ultraviolet absorption cross sections and reaction kinetics and mechanisms for peroxy radicals in the gas phase. Chemical Reviews 92, 667–710.

Wallington T.J., Hurley, M.D., Schneider, W.F., 1996. Atmospheric chemistry of CH_3Cl: mechanistic study of the reaction of CH_2ClO_2 radicals with HO_2. Chemical Physics Letters 251, 164–173.

Wallington T.J., Nielsen O.J., Sehested J., 1997. Reactions of Organic Peroxy Radicals in the Gas Phase. In: Alfassi, Z.B. (Eds.), Peroxyl Radicals, Wiley, New York, pp. 81–112.

Wei W.-M., Zheng R.-H., 2007. Theoretical study on the reaction mechanism of CH_2ClO_2 with HO_2. Journal of Molecular Structure. THEOCHEM 812, 1-11.

Wilson A.K., van Mourik T., Dunning T.H., 1996. Gaussian basis sets for use in correlated molecular calculations. VI. Sextuple zeta correlation consistent basis sets for boron through neon. Journal of Molecular Structure: THEOCHEM 388, 339–349.

Woon D.E., Dunning Jr., T.H., 1993. Gaussian basis sets for use in correlated molecular calculations. III. The atoms aluminium through argon. Journal of Chemical Physics 98 1358–1372.

Yang X, Cox R.A., Warwick N.J., Pyle J.A., Carver G.D., O'Connor F.M., Savage N.H., 2006. Tropospheric bromine chemistry and its impact on ozone: A model study. Journal of Geophysical Research 110 (D23311). doi: 10.1029/2005JD006244.

Yokouchi Y., Hasebe F., Fujiwara M., Takashima H., Shiotani M., Nishi N., Kanaya Y., Hashimoto S., Fraser P., Toom-Sauntry D., Mukai H., and Nojiri Y., 2005. Correlations and emission ratios among bromoform, dibromochloromethane, and dibromomethane in the atmosphere. Journal of Geophysical Research 110 (D23309). doi:10.1029/2005JD006303.

Table 1: Standard reaction enthalpies at 298 K calculated at the CCSD(T)/aug-cc-pVTZ//MP2/cc-pVTZ level of theory with and without the cf-correction involved in the reaction between the brominated methyl peroxy radicals and HO_2.

Reaction[a]		$\Delta_r H°_{298K}$ (kcal mol^{-1})		
		This work[b]	McGivern et al. (2004)	analogous chlorinated compounds (Hou et al., 2005)
$CBr_3O_2 + HO_2 \rightarrow CBr_3O_2H + O_2$	6a	-44.3 (-44.2)	-44.2	-44.2
$CBr_3O_2 + HO_2 \rightarrow CBr_2O + HOBr + O_2$	6b	-77.2 (-77.2)		-71.8
$CBr_3O_2 + HO_2 \rightarrow CBr_3O + OH + O_2$	6b'	-3.7 (-3.6)	-6.5	-6.2
$CHBr_2O_2 + HO_2 \rightarrow CHBr_2O_2H + O_2$	20a	-43.5 (-43.4)	-43.8	-43.6
$CHBr_2O_2 + HO_2 \rightarrow CHBrO + HOBr + O_2$	20b	-68.2 (-68.2)		-63.2
$CHBr_2O_2 + HO_2 \rightarrow CHBr_2O + OH + O_2$	20b'	-0.3 (-0.2)	-2.7	-5.5
$CHBr_2O_2 + HO_2 \rightarrow CBr_2O + H_2O + O_2$	20c	-107.7 (-107.0)		-109.9
$CH_2BrO_2 + HO_2 \rightarrow CH_2BrO_2H + O_2$	35a	-42.7 (-42.6)	-39.2	-42.7
$CH_2BrO_2 + HO_2 \rightarrow CH_2O + HOBr + O_2$	35b	-55.0 (-54.1)		-47.7
$CH_2BrO_2 + HO_2 \rightarrow CH_2BrO + OH + O_2$	35b'	1.3 (1.4)	1.6	-5.8
$CH_2BrO_2 + HO_2 \rightarrow CHBrO + H_2O + O_2$	35c	-101.7 (-101.1)		-103.6

[a] The molecular oxygen is in its electronic ground state.

[b] the values in parentheses correspond to the CCSD(T)/aug-cc-pVTZ energies without the cf-correction.

Table 2: Comparisons of well-known Henry's law constants (mol L^{-1} atm^{-1}) (referenced by Sander et al. 1999) with estimated Henry's law constants using the two methods, Bond Contribution Method (BCM) and Molecular Connectivity Index method (MCI).

	BCM	MCI	Experimental (Sander et al., 1999)
Aldehydes			
CH_3CHO	15	15	17
C_2H_5CHO	11	12	13
C_4H_9CHO	4.8	7.5	6.4
Ketones			
CH_3COCH_3	20	18	27
$C_2H_5COCH_3$	15	15	20
Peroxides			
CH_3O_2H	147	1501	310
$C_2H_5O_2H$	110	1327	340
$OHCH_2O_2H$	4.0×10^6	7.5×10^6	1.7×10^6
Alcohols			
CH_3OH	235	195	230
C_2H_5OH	176	167	160
C_3H_7OH	132	131	130
Compounds with bromine			
$CHBr_3$	8.9	2.4	2.1
CH_2Br_2	1.0	1	1.1
$C_2H_4Br_2$	0.8	0.8	1.5

Table 3: Henry's law constants ($k°_H$) of the intermediate products gases (PGs).

Species	$k°_H$ (298 K) (mol L^{-1} atm^{-1})
HBr	0.71 [a]
HOBr	6.1×10^3 [a]
CBr_3O_2H	1.9×10^5 [b]
$CHBr_2O_2H$	2.24×10^4 [b]
CH_2BrO_2H	2.58×10^3 [b]
CHBrO	74 [c]
CBr_2O	21.5 [c]
$CBr_3O_2NO_2$	401 [b]
$CHBr_2O_2NO_2$	304 [b]
$CH_2BrO_2NO_2$	35 [b]
CBr_3OH	1.5×10^5 [b]
$CHBr_2OH$	1.73×10^4 [b]
CH_2BrOH	2.0×10^3 [b]

[a] Sander et al., 1999.

[b] Bond Contribution Method (BCM: Meylan and Howard, 1991).

[c] Molecular Connectivity Index (MCI: Nirmalakhandan and Speece, 1988).

Table 4: Summary of the kinetic data used for the degradation of bromoform.

N°	Reactions	Rate constants (cm^3 molecule^{-1} s^{-1})	Comments	References
1	$CHBr_3 + OH$	1.35×10^{-12} exp(-600/T)		Sander et al.(2011)
3	$CHBr_3 + Cl$	4.85×10^{-12} exp(-850/T)		Kambanis et al. (1997)
16	$CHBr_3 + h\nu$		Absorption Cross Section	Sander et al.(2011)
4	$CBr_3O_2 + NO$	7.3×10^{-12} exp(270/T)	From k($CCl_3O_2 + NO$)	Dognon et al. (1985)
5	$CBr_3O_2 + NO_2$	$k_0=2.9\times10^{-29}$ (T/300)$^{-6.8}$ $k_\infty=1.3\times10^{-11}$ (T/300)$^{-1}$	From k($CCl_3O_2 + NO_2$)	Caralp et al. (1988)
6	$CBr_3O_2 + HO_2$	4.8×10^{-13}exp(706/T)	From k($CCl_3O_2 + HO_2$) Branching ratio section 2.3.1	Catoire et al. (1996)
7	$CBr_3O_2 + CH_3O_2$	6.6×10^{-12}	k($CCl_3O_2 + CH_3O_2$) at 298 K, assumed constant with temperature	Catoire et al. (1996)
17	$CHBr_2O_2 + NO$	3.81×10^{-12}exp(360/T)	From k($CHCl_2O_2 + NO$) (from k($RO_2 + NO$)×1.5)	Jenkin et al. (1997)
19	$CHBr_2O_2 + NO_2$	2.9×10^{-29} (T/300)$^{-6.8}$ 1.3×10^{-11} (T/300)$^{-1}$	From k($CCl_3O_2 + NO_2$)	Caralp et al. (1988)
20	$CHBr_2O_2 + HO_2$	5.6×10^{-13}exp(700/T)	From k($CHCl_2O_2 + HO_2$) Branching ratio section 2.3.2	Catoire et al. (1996)
21	$CHBr_2O_2 + CH_3O_2$	1.2×10^{-12}	k($CHCl_2O_2 +CH_3O_2$) at 298 K, assumed constant with temperature	Shallcross et al. (2005)
10	$CBr_2O + h\nu$		Absorption Cross Section	Sander et al.(2011)
11	$CBr_3O_2NO_2 + M$	$k_0=6.3\times10^{-3}$ exp(-10235/T)[N_2] $k_\infty=1.42\times10^{16}$exp(-1500/T)	From k($CCl_3O_2NO_2$+M)	Köppenkastrop and Zabel (1991)
12	$CBr_3O_2NO_2 + h\nu$		Absorption Cross Section of $CH_3O_2NO_2$	Atkinson et al. (2006)
13	$CBr_3O_2H + h\nu$		Absorption Cross Section of CH_3O_2H	Vaghjiani and Ravishankara (1989)
14	$CBr_3O_2H +OH$	1.9×10^{-12}exp(190/T)	From $RO_2H + OH$	Jenkin et al. (1997)
23	$CHBrO + h\nu$		Absorption Cross Section	Sander et al.(2011)
24	$CHBr_2O_2NO_2 + M$	$k_0=6.3\times10^{-3}$ exp(-10235/T)[N_2] $k_\infty=1.42\times10^{16}$exp(-1500/T)	From k($CCl_3O_2NO_2$+M)	Köppenkastrop and Zabel (1991)
25	$CHBr_2O_2NO_2 + h\nu$		Absorption Cross Section of $CH_3O_2NO_2$	Atkinson et al. (2006)
26	$CHBr_2O_2H + h\nu$		Absorption Cross Section of CH_3O_2H	Vaghjiani and Ravishankara (1989)
27	$CHBr_2O_2H + OH$	1.9×10^{-12}exp(190/T)	From $RO_2H + OH$	Jenkin et al. (1997)
15	CBr_3OH+OH	3.6×10^{-14}	k($CCl_3O_2 + OH$) at 298 K, assumed constant with temperature	Jenkin et al. (1997)
28	$CHBr_2OH+OH$	9.34×10^{-13}	k($CHCl_2O_2 + OH$) at 298 K, assumed constant with temperature	Jenkin et al. (1997)

Table 5: Summary of the kinetic data used for the degradation of dibromomethane.

N°	Reactions	Rate constants $(cm^3.molecule^{-1}.s^{-1})$	Comments	References
29	$CH_2Br_2 + OH$	$2 \times 10^{-12} \exp(-840/T)$		Sander et al.(2011)
30	$CH_2Br_2 + Cl$	$6.3 \times 10^{-12} \exp(-800/T)$		Sander et al.(2011)
31	$CH_2Br_2 + h\nu$		Absorption Cross Section	Sander et al.(2011)
17	$CHBr_2O_2 + NO$	$3.81 \times 10^{-12} \exp(360/T)$	From $k(CHCl_2O_2 + NO)$ (from $k(RO_2 + NO) \times 1.5$)	Jenkin et al. (1997)
19	$CHBr_2O_2 + NO_2$	$9.2 \times 10^{-29} (T/300)^{-6}$ $1.5 \times 10^{-11} (T/300)^{-0.7}$	From $k(CCl_3O_2 + NO_2)$	Caralp et al. (1988)
20	$CHBr_2O_2 + HO_2$	$5.6 \times 10^{-13} \exp(700/T)$	From $k(CHCl_2O_2 + HO_2)$ Branching ratio section 2.4.2	Catoire et al. (1996)
21	$CHBr_2O_2 + CH_3O_2$	1.2×10^{-12}	From $k(CHCl_2O_2 + CH_3O_2)$ at 298 K, assumed constant with temperature	Shallcross et al. (2005)
32	$CH_2BrO_2 + NO$	$4 \times 10^{-12} \exp(300/T)$	Temperature dependence from $k(RO_2 + NO)$	Sander et al.(2011)
34	$CH_2BrO_2 + NO_2$	$9.2 \times 10^{-29} (T/300)^{-6}$ $1.5 \times 10^{-11} (T/300)^{-0.7}$	From $k(CCl_3O_2 + NO_2)$	Caralp et al. (1988)
35	$CH_2BrO_2 + HO_2$	$3.3 \times 10^{-13} \exp(822/T)$	From $k(CH_2ClO_2 + HO_2)$ Branching ratio section 2.3.2	Catoire et al. (1994)
36	$CH_2BrO_2 + CH_3O_2$	2.51×10^{-12}	From $k(CH_2ClO_2 + CH_3O_2)$ At 298 K, assume constant with temperature	Villenave et al. (1996)
22	$CBr_2O + h\nu$		Absorption Cross Section	Sander et al.(2011)
38	$CH_2BrO_2NO_2 + M$	$k_0 = 6.3 \times 10^{-3} \exp(-10235/T)[N_2]$ $k_\infty = 1.42 \times 10^{16} \exp(-1500/T)$	From $k(CCl_3O_2NO_2 + M)$	Köppenkastrop and Zabel (1991)
39	$CH_2BrO_2NO_2 + h\nu$		Absorption Cross Section of $CH_3O_2NO_2$	Atkinson et al. (2006)
40	$CH_2BrO_2H + h\nu$		Absorption Cross Section of CH_3O_2H	Vaghjiani and Ravishankara (1989)
41	$CH_2BrO_2H + OH$	$1.9 \times 10^{-12} \exp(190/T)$	From $RO_2H + OH$	Jenkin et al.(1997)
23	$CHBrO + h\nu$		Absorption Cross Section	Sander et al.(2011)
24	$CHBr_2O_2NO_2 + M$	$k_0 = 6.3 \times 10^{-3} \exp(-10235/T)[N_2]$ $k_\infty = 1.42 \times 10^{16} \exp(-1500/T)$	From $k(CCl_3O_2NO_2 + M)$	Köppenkastrop and Zabel (1991)
25	$CHBr_2O_2NO_2 + h\nu$		Absorption Cross Section of $CH_3O_2NO_2$	Atkinson et al. (2006)
26	$CHBr_2O_2H + h\nu$		Absorption Cross Section of CH_3O_2H	Vaghjiani and Ravishankara (1989)
27	$CHBr_2O_2H + OH$	$1.9 \times 10^{-12} \exp(190/T)$	From $RO_2H + OH$	Jenkin et al.(1997)
42	$CH_2BrOH + OH$	1.8×10^{-12}	From $k(CH_2ClO_2 + OH)$ at 298 K, assumed constant with temperature	Jenkin et al.(1997)

| 28 | CHBr$_2$OH+OH | 9.34×10^{-13} | From k(CHCl$_2$O$_2$ + OH) at 298 K, assumed constant with temperature | Jenkin et al. (1997) |

Table 6: Initial volume mixing ratios in parts per billion (ppbv) used in the model for the two simulation scenarios, from MOCAGE CTM outputs (see text for details).

Model Parameter at 1000 m	Scenario	
	CLEAN	MODERATE
O$_3$	26	29
NO$_x$	0.036	0.061
HNO$_3$	0.78	2.5
CO	62	64
CH$_4$	1590	1557

Table 7: Reactions tested in the different simulations for $CHBr_3$.

Simulation	Scenario	$CHBr_3$ initialization	RO_2+ NO_2	RO_2+ CH_3O_2	$RO_2 + HO_2$		
					(a)	(b)	(c)
Reference	CLEAN and MODERATE	Fig. 2A and 2B	included	included	1 [a] 0.7 [b]	0 [a] 0 [b]	/ 0.3 [b]
#1	CLEAN and MODERATE	Fig. 2B	not included	included	1 [a] 0.7 [b]	0 [a] 0 [b]	/ 0.3 [b]
#2	CLEAN	Fig. 2B	not included	not included	1 [a] 0.7 [b]	0 [a] 0 [b]	/ 0.3 [b]
#3	CLEAN	Fig. 2B	not included	not included	0.5 [a] 0.5 [b]	0.5 [a] 0.5 [b]	/ 0 [b]

(a), (b), (c): branching ratios for the channels of $RO_2 + HO_2$ reaction as defined in Table 1 or Fig. 1.

/: Channel not possible

[a]*: $RO_2 = CBr_3O_2$*

[b]*: $RO_2 = CHBr_2O_2$*

Table 8: Reactions tested in the different simulations for CH_2Br_2.

n°	Scenario	RO_2+NO_2	$RO_2+CH_3O_2$	$RO_2 + HO_2$		
				(a)	(b)	(c)
Ref	CLEAN and MODERATE	included	included	0.7^a	0^a	0.3^a
				0.2^b	0^b	0.8^b
#1	CLEAN	included	included	0.7^a	0^a	0.3^a
				0.9^b	0^b	0.1^b

(a), (b), (c): branching ratios for the channels of $RO_2 + HO_2$ reaction as defined in Table 1 and Fig. 1.

/: Channel not possible

[a]: $RO_2 = CHBr_2O_2$

[b]: $RO_2 = CH_2BrO_2$

Table 9: Relative partitioning of Br atom at the end of the simulation (i.e. after 10 days), at 1 km altitude, in $CHBr_3$ degradation for the source gas, organic and inorganic species: for the reference simulation, simulation #2 and simulation #3 in the clean atmosphere and for the reference simulation in the moderately polluted atmosphere (for the simulation conditions, see Tables 6 and 7).

	Clean atmosphere			Moderate pollution
	Reference simulation	Simulation # 2	Simulation # 3	Reference simulation
Source gas				
$CHBr_3$	37.5 %	40.9 %	40.9 %	31 %
Organic products	17.1 %	16.3 %	12.9 %	19.2 %
CBr_2O	11.8 %	12.8 %	9.6 %	15.3 %
$CHBrO$	1.4 %	1.5 %	1.9 %	1.3 %
CBr_3O_2H	0.6 %	1.0 %	0.6 %	0.4 %
$CHBr_2O_2H$	0.8 %	1.0 %	0.8 %	0.3 %
CBr_3OH	2.3 %	/	/	1.8 %
$CHBr_2OH$	0.2 %	/	/	0.1 %
CBr_3O_2	< 0.01 %	< 0.01 %	< 0.01 %	< 0.01 %
$CHBr_2O_2$	< 0.01 %	< 0.01 %	< 0.01 %	< 0.01 %
$CBr_3O_2NO_2$	< 0.01 %	/	/	< 0.01 %
$CHBr_2O_2NO_2$	< 0.01 %	/	/	< 0.01 %
Inorganic products	45.3 %	42.9 %	46.1 %	49.9 %
HBr	36 %	33.5 %	36.1 %	23.5 %
BrO	1.1 %	1.0 %	1.0 %	1.6 %
HOBr	3.0 %	2.9 %	3.1 %	5.2 %
$BrONO_2$	5.1 %	5.4 %	5.8 %	19.5 %
Br	0.1 %	0.1 %	0.1 %	0.1 %
Br_{max}[a] (pptv)	22.5 % (0.9 – 9.3) (Fig. 2A – 2B)	23.7 % (10.3) (Fig. 2B)	21.5 % (8.8) (Fig. 2B)	43 % (1.6 – 17.7) (Fig. 2A – 2B)

[a]: Maximum Br (in %) potentially able to reach the tropical tropopause layer (TTL).

Table 10: Relative partitioning of Br atom at the end of the simulation (i.e. after 50 days), at 1 km altitude, in CH_2Br_2 degradation for the source gas, organic and inorganic species: for the reference simulation in clean atmosphere and for the reference simulation in polluted atmosphere (for the simulation conditions, see Table 8).

	Clean atmosphere	Moderate pollution
	Reference simulation	Reference simulation
Source gas		
CH_2Br_2	54.4 %	39.5 %
Organic products		
CBr_2O	1.0 %	1.0 %
CHBrO	0.3 %	0.3 %
$CHBr_2O_2H$	0.3 %	0.2 %
$CHBr_2OH$	0.1 %	0.1 %
Inorganic products		
HBr	36.3 %	40.1 %
BrO	1.5 %	2.8 %
HOBr	3.3 %	8.6 %
$BrONO_2$	2.6 %	7.4 %
Br	0.1 %	0.1 %
Br_{max}[a] (pptv)	8.8 % (0.19)	20.2 % (0.42)

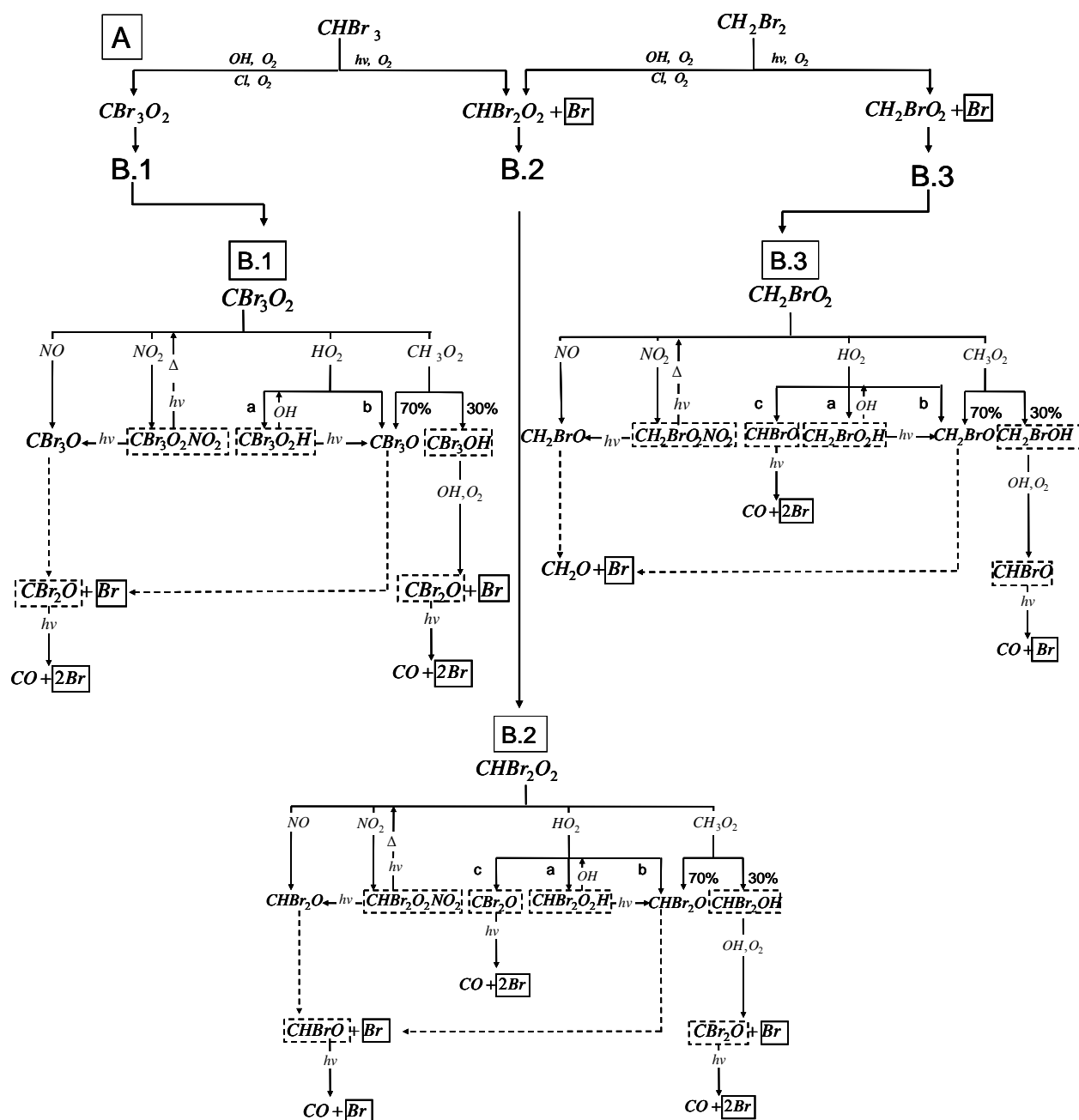[a]: Maximum Br (in %) potentially able to reach the TTL.

Fig. 1: Chemical mechanisms of bromoform ($CHBr_3$) and dibromomethane (CH_2Br_2) degradations. A: Initial steps reaction (OH, Cl and photolysis). B: Brominated peroxy radical reaction degradation mechanism, B.1: CBr_3O_2, B.2: $CHBr_2O_2$ (common to both molecules) and B.3: CH_2BrO_2. Stable intermediate products are enclosed in dotted line boxes and final inorganic bromine inside full line boxes. The decomposition reactions are indicated by dashed arrows.
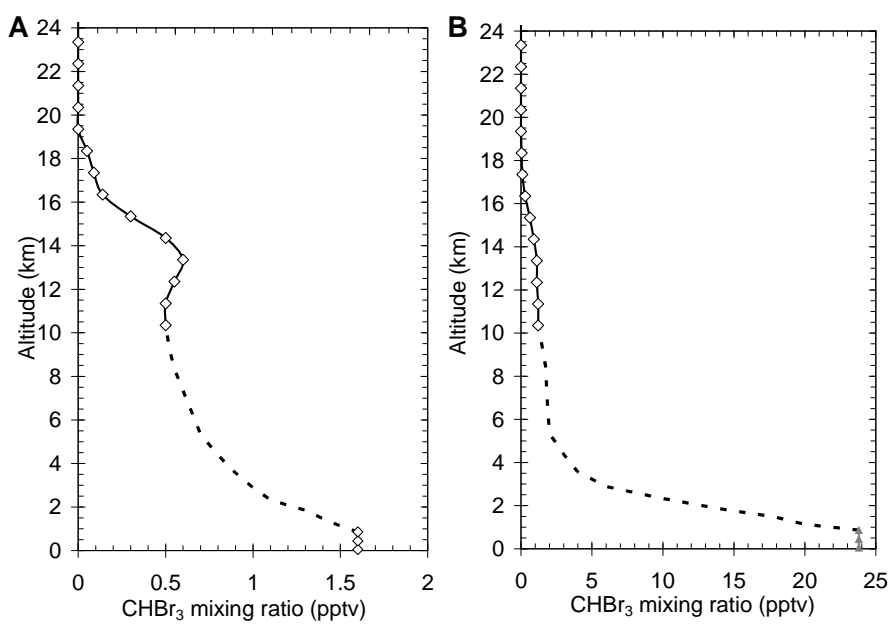
Fig. 2: Bromoform vertical profiles used for the initialization of the simulations (see Section 3). A: mean tropical data, and B: maximum tropical data, given by Montzka and Reimann et al. (2011; open diamonds), Yokouchi et al. (2005; full triangles) and Hossaini et al. (2010; dashed lines).

Fig. 3: Dibromomethane vertical profile used for the initialization of the simulations (see Section 3) from Montzka and Reimann et al. (2011; open diamonds) and dashed line is an interpolation from observed mixing ratio profiles (Hossaini et al., 2010).

Fig. 4: $CHBr_3$ total lifetime τ_{total} (bold line) in the overall simulated domain due to the reaction with OH (dot-dashed line) and due to the photolysis (dotted line) in the clean atmosphere (left panel) and in the moderately polluted atmosphere (right panel).

Fig. 5: 10-days simulation average for OH vertical profiles (molecules cm^{-3}) in the clean atmosphere (full line) and in the moderately polluted atmosphere (dashed line).

Fig. 6: Vertical profiles of Br contained in $CHBr_3$ (top), in the total organics (upper middle), in HBr (lower middle), and in the total inorganics (bottom) except HBr, on 17 November (open circle), on 20 November (open square), on 23 November (cross) and on 26 November (open triangle), for the clean atmosphere (left panels) and the polluted atmosphere (right panels) for the bromoform initialization from Fig. 2A.

Fig. 7: Time dependence of Br partitioning between the most soluble species (CBr_3O_2H, $CHBr_2O_2H$, CBr_3OH, $CHBr_2OH$, HBr) and the least soluble species (BrO, $BrONO_2$, Br, HOBr, CBr_2O, CHBrO, $CBr_3O_2NO_2$ and $CHBr_2O_2NO_2$) for the reference simulation (see Table 7) in the clean atmosphere (top panels) and in the polluted atmosphere (bottom panels). A: $CHBr_3$ initialization from Fig. 2A (Montzka and Reimann et al., 2011), and B: $CHBr_3$ initialization from Fig. 2B (Yokouchi et al., 2005 and Montzka and Reimann et al., 2011)).

Fig. 8: Simplified chemical mechanism of bromoform ($CHBr_3$) and dibromomethane (CH_2Br_2) degradations. Stable intermediate products are enclosed in dashed line boxes for the

least soluble species, in dotted line boxes for the most soluble species, and the final inorganic bromine in full line boxes.

Fig. 9: Vertical profiles of Br contained in CH_2Br_2 (top), in the total organics (upper middle), in HBr (lower middle) and in the total inorganics (bottom) except HBr on 17 November (open circle), on 03 December (open square), on 20 December (cross) and on 05 January (open triangle), for the clean atmosphere (left panels) and the polluted atmosphere (right panels).

Fig. 10: Time dependence of Br partitioning between the most soluble species ($CHBr_2O_2H$, CH_2BrO_2H, $CHBr_2OH$, CH_2BrOH, HBr) and the least soluble species (BrO, $BrONO_2$, Br, HOBr, CBr_2O, CHBrO, $CHBr_2O_2NO_2$ and $CH_2BrO_2NO_2$) for the reference simulation in the clean atmosphere (left panel) and in the polluted atmosphere (right panel).

Fig. 1: Chemical mechanisms of bromoform (CHBr₃) and dibromomethane (CH₂Br₂) degradations. A: Initial steps reaction (OH, Cl and photolysis). B: Brominated peroxy radical reaction degradation mechanism, B.1: CBr₃O₂, B.2: CHBr₂O₂ (common to both molecules) and B.3: CH₂BrO₂. Stable intermediate products are enclosed in dotted line boxes and final inorganic bromine inside full line boxes. The decomposition reactions are indicated by dashed arrows.

Fig. 2: Bromoform vertical profiles used for the initialization of the simulations (see Section 3). A: mean tropical data, and B: maximum tropical data, given by Montzka and Reimann et al. (2011; open diamonds), Yokouchi et al. (2005; full triangles) and Hossaini et al. (2010; dashed lines).

Fig. 3: Dibromomethane vertical profile used for the initialization of the simulations (see Section 3) from Montzka and Reimann et al. (2011; open diamonds) and dashed line is an interpolation from observed mixing ratio profiles (Hossaini et al., 2010).

Fig. 4: CHBr$_3$ total lifetime τ_{total} (bold line) in the overall simulated domain due to the reaction with OH (dot-dashed line) and due to the photolysis (dotted line) in the clean atmosphere (left panel) and in the moderately polluted atmosphere (right panel).

Fig. 5: 10-days simulation average for OH vertical profiles (molecules cm^{-3}) in the clean atmosphere (full line) and in the moderately polluted atmosphere (dashed line).

Fig. 6: Vertical profiles of Br contained in CHBr$_3$ (top), in the total organics (upper middle), in HBr (lower middle), and in the total inorganics (bottom) except HBr, on 17 November (open circle), on 20 November (open square), on 23 November (cross) and on 26 November (open triangle), for the clean atmosphere (left panels) and the polluted atmosphere (right panels) for the bromoform initialization from Fig. 2A.

Fig. 7: Time dependence of Br partitioning between the most soluble species (CBr_3O_2H, $CHBr_2O_2H$, CBr_3OH, $CHBr_2OH$, HBr) and the least soluble species (BrO, $BrONO_2$, Br, HOBr, CBr_2O, CHBrO, $CBr_3O_2NO_2$ and $CHBr_2O_2NO_2$) for the reference simulation (see Table 7) in the clean atmosphere (top panels) and in the polluted atmosphere (bottom panels). A: $CHBr_3$ initialization from Fig. 2A (Montzka and Reimann et al., 2011), and B: $CHBr_3$ initialization from Fig. 2B (Yokouchi et al., 2005 and Montzka and Reimann et al., 2011)).
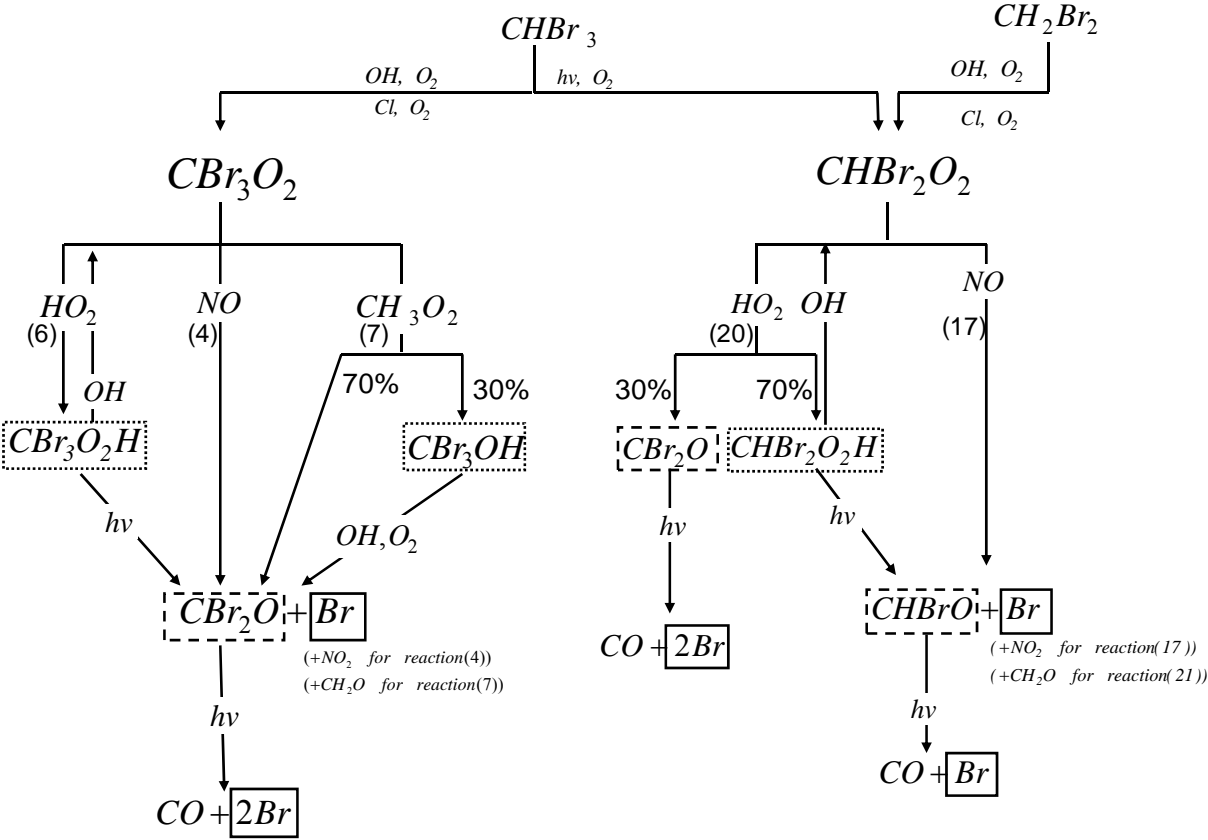
Fig. 8: Simplified chemical mechanism of bromoform (CHBr$_3$) and dibromomethane (CH$_2$Br$_2$) degradations. Stable intermediate products are enclosed in dashed line boxes for the least soluble species, in dotted line boxes for the most soluble species, and the final inorganic bromine in full line boxes.
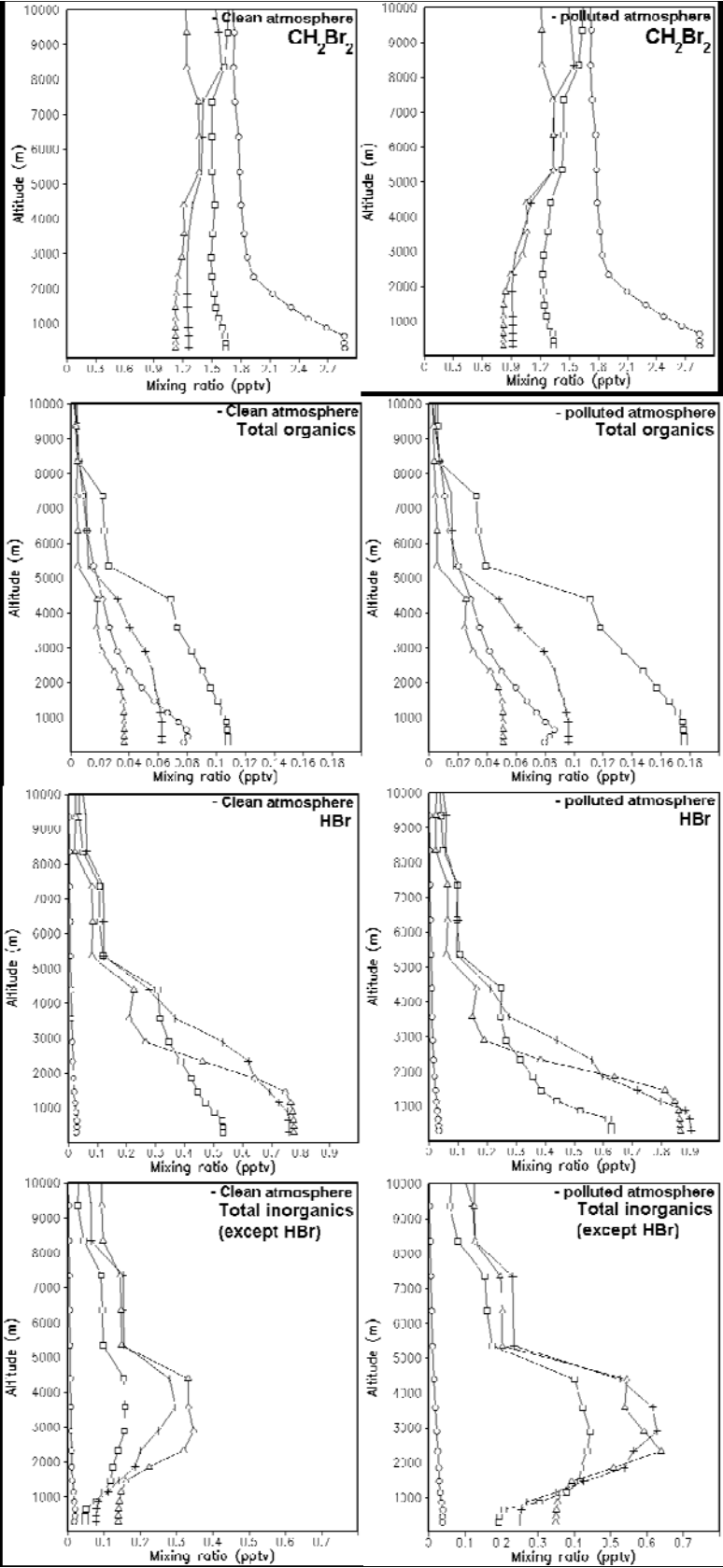
Fig. 9: Vertical profiles of Br contained in CH_2Br_2 (top), in the total organics (upper middle), in HBr (lower middle) and in the total inorganics (bottom) except HBr on 17 November (open circle), on 03 December (open square), on 20 December (cross) and on 05 January (open triangle), for the clean atmosphere (left panels) and the polluted atmosphere (right panels).
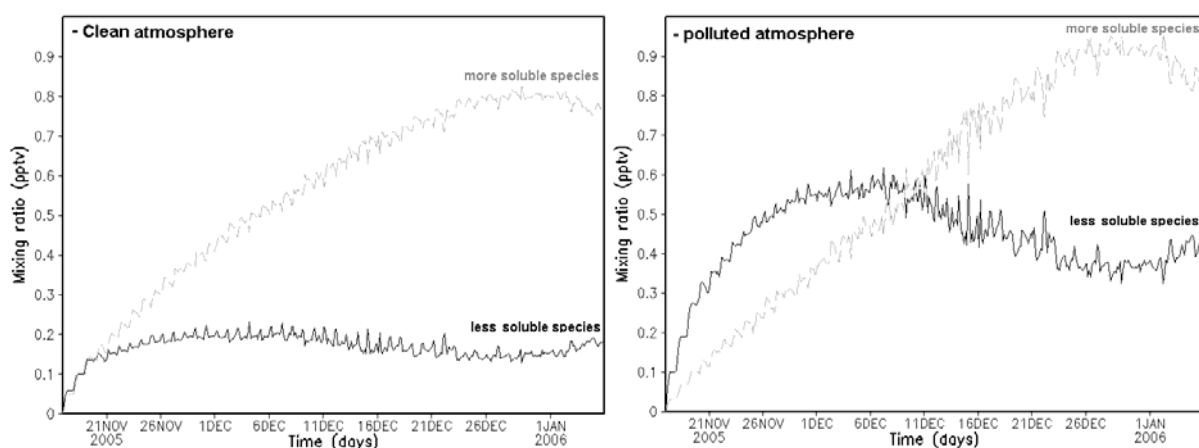
Fig. 10: Time dependence of Br partitioning between the most soluble species (CHBr$_2$O$_2$H, CH$_2$BrO$_2$H, CHBr$_2$OH, CH$_2$BrOH, HBr) and the least soluble species (BrO, BrONO$_2$, Br, HOBr, CBr$_2$O, CHBrO, CHBr$_2$O$_2$NO$_2$ and CH$_2$BrO$_2$NO$_2$) for the reference simulation in the clean atmosphere (left panel) and in the polluted atmosphere (right panel).